Solar Energy Materials & Solar Cells 95 (2011) 1785–1799

Contents lists available at ScienceDirect

Solar Energy Materials & Solar Cells

journal homepage: www.elsevier.com/locate/solmat

Recent development of the inverted configuration organic solar cells

Fujun Zhang [a,*], Xiaowei Xu [a], Weihua Tang [b,**], Jian Zhang [c], Zuliang Zhuo [a], Jian Wang [a], Jin Wang [a], Zheng Xu [a], Yongsheng Wang [a]

[a] Key Laboratory of Luminescence and Optical Information (Ministry of Education of China), School of Science, Beijing Jiaotong University, Beijing 100044, People's Republic of China
[b] Key Laboratory of Soft Chemistry and Functional Materials (Ministry of Education of China), College of Chemical Engineering, Nanjing University of Science and Technology, Nanjing 210094, People's Republic of China
[c] State Key Laboratory of Catalysis, Dalian Institute of Chemical Physics, 457 Zhongshan Road, Dalian 116023, People's Republic of China

ARTICLE INFO

Article history:
Received 14 December 2010
Received in revised form
30 January 2011
Accepted 1 February 2011
Available online 3 March 2011

Keywords:
Organic solar cells
Inverted configuration
Power conversion efficiency
Stability
Degrade mechanism

ABSTRACT

Recent years, the power conversion efficiency (PCE) of normal configuration organic solar cells (OSCs) has obtained rapid progress to reach more than 6% under standard illumination, which is reasonable value for the commercial criterion. More and more research attention has been paid on the stability and lifetime of OSCs. A novel structural OSCs with high work function metal or metal oxide as the top electrode and low work function metal as the bottom anode is proposed and named as inverted configuration OSCs. The inverted configuration OSCs with high work function metal as top cathode could improve OSCs's lifetime, i.e., protecting cells from the damage by oxygen and moisture in air. Furthermore, the inverted configuration OSCs is the appealing alternative to the conventional regular structure due to the inherent vertical phase separation in the polymer active layers and high stability or long device lifetime. The inverted configuration OSCs have not only achieved an impressive PCE of 4.4%, but also exhibited an exceptional device lifetime without encapsulation. In this review article, the recent developments and vital researches on the inverted configuration OSCs are summarized.

1. Introduction

Recent years, more and more research attention has been paid to the development of organic solar cells (OSCs) due to its rapid efficiency improvement, the cost effective energy harvesting, ease of processing, and compatibility with flexible substrates. The power conversion efficiency (PCE) of polymer solar cells has reached as high as ~6% [1,2]. Many effective approaches have been carried out to improve the performance of solar cells through the synthesis of new narrow bandgap materials for better photon harvesting, optimization of phase segregation in the bulk heterojunction (BHJ) layers, interfacial modification for better charge carrier collection, and design of novel configuration cells [3–8]. However, many basic physical and mechanical problems, such as the interfacial states between organic electron donor/acceptor, between organic materials/inorganic semiconductor, and between organic materials/metal, stability/degradation of cells, morphology control, and the role of ultrathin interlayer, are still not very clear [9–20]. The current research pursuits for OSCs concentrate in obtaining high efficiency, stability, low-cost and high-speed production in individual cells. The ultimate realization of all these goals in one single cell is a great challenge and no such report has been published. In order to improve the PCE of OSCs, the key parameters, such as short circuit current (J_{sc}), open circuit voltage (V_{oc}), Fill factor (FF), series and shunt resistance, should be optimized by improving the photon harvesting, interfacial engineering and different treatments on substrates or active layers.

The normal configuration OSCs are made of an active BHJ layer or planner heterojunction layers sandwiched by a high work function and transparent metal oxide as the bottom anode and a low work function metal as the top cathode. For efficient charge collection, work functions of anode and cathode should be matched to the highest occupied molecular orbits (HOMO) of donor and the lowest unoccupied molecular orbits (LUMO) of acceptor, respectively. Low work function metals as the top cathode have been selected for better matching with the LUMO of acceptor. However, metals with low work function are not very stable as the top electrode due to their sensitivity to oxygen and moisture in air [21,22]. In order to protect top electrode, bi-layered metals such as Ca/Al or Mg/Al have been used as composite cathode for the performance improvement in OSCs and organic light-emitting diodes (OLEDs) [23,24]. Inverted configuration OSCs with low work function metals modified ITO as the transparent cathode and a high work function metal as anode could effectively avoid the device degradation induced by the

* Corresponding author. Tel.: +86 010 51688605; fax: +86 010 51683933.
** Corresponding author. Tel./fax: +86 025 84317311.
E-mail addresses: fjzhang@bjtu.edu.cn (F. Zhang), whtang@mail.njust.edu.cn (W. Tang).

0927-0248/$ - see front matter © 2011 Elsevier B.V. All rights reserved.
doi:10.1016/j.solmat.2011.02.002

contamination of metal cathodes. The inverted configuration OSCs also avoids the need for using poly (styrene sulfonic acid) doped poly (3,4-ethylenedioxythiophene) PEDOT:PSS at ITO interface, which has been shown to degrade performance due to the effect of strong acidic nature of PSS on the ITO surface [25]. The common used high work function metal electrodes like Ag and Au are effective in hole collection; however, the work function of Au may decrease from 5.4 to 4.7 eV in the air due to the contamination by carbon and oxide, which will lead to the degradation of the device's performance [26]. Nevertheless, in the case of the Ag electrode, the oxidization of Ag will increase its work function to from 4.3 to 5.0 eV, which will benefit for hole collection from electron donor materials to Ag and improve the cell's performance [27]. It is also expected that the inverted configuration has the advantage over the normal configuration because of the P3HT:PCBM vertical phase separation [28]. The vertical phase separation is attributed to the surface energy difference of the components and their interactions with the substrates. This inhomogeneous distribution of the donor and acceptor components significantly affects normal configuration OSCs performance and makes the inverted configuration OSCs as a promising choice. Recent years, the efficiency gap between normal and inverted structural solar cells has been rapidly dwindled. Yang' group reported that the efficiency of inverted configuration OSCs has more than 4% under standard measurement conditions [29]. Recently, Hsieh et al. [30] reported that an inverted configuration OSCs has not only achieved an impressive PCE of 4.4%, but also exhibited an exceptional device lifetime without encapsulation.

The ideal fabrication process for OSCs will be solution processing, in which different cell layers are deposited onto flexible substrates to tailor for the ultimate simple roll-to-roll type printing. Additionally, the OSCs should maintain high device stability and efficiency over a certain period of time. The inverted configuration OSCs may be the best candidate to meet all these requirements including high efficiency, stability, low-cost and high-speed production into one system. Recently, the inverted device architecture has been investigated as a suitable architecture tailoring for solution processing, which allows various cell layers to deposit onto flexible substrates and is promising for scale-up production via industrial roll-to-roll type fabrication.

This review article is organized as follows: following a brief introduction on the mechanism of OSCs in Section 2. An overview of commonly used materials is provided in Section 3. Section 4 is devoted to introduce the latest achievement on the inverted configuration OSCs and discuss the probable routes for efficiency improvement of inverted configuration OSCs. Finally, we conclude and offer our perspective on the challenges to achieve high efficiency and long device lifetime in Section 6.

2. Operational mechanism

Organic solar cells have attracted a significant amount of attention due to the need to develop an inexpensive clean and sustainable renewable energy source. No matter what the cell structures are, the operational mechanism is the same. Inverted configuration is mainly directed to solve the issue of device lifetime and stability. The operation of OSCs mainly involves the following five steps: (i) the light absorption by the active layer; (ii) the formation of exciton and subsequent diffusion to the interface of donor and acceptor; (iii) the exciton dissociation into the electrons and holes; (iv) free charge carriers transport in their individual pathway or layer; and (v) charge extraction by their corresponding electrodes. One of the integrative targets valuating the performance of OSCs is PCE, which is strongly determined by the following key parameters, namely V_{oc}, J_{sc}, *FF*, series and shunt resistance. The V_{oc} of a solar cell is defined as the voltage which compensates the current flow through the external circuit. The J_{sc} is defined as the current during the external circuit without applied voltage. FF is a more sensitive parameter in comparison to V_{oc} and J_{sc}, and depends on the mobility (μ)–lifetime (τ) product of the bulk materials, thickness of the active layer and morphology of interface between cathode/active layer [31]. As such, many researches have been conducted on interface engineering by inserting different ultra thin layers to increase the performance of OSCs [22–30]. An ideal solar cell should have low series resistance (R_s) and high shunt resistance (R_{sh}) in order to optimize the performance of device. The R_s reflects the Ohmic loss in the entire device, a combination of the contact resistance and charge transfer rate at the interfaces as well as the bulk resistance of the active materials. The R_{sh} is related to the loss of charge carriers due to current leakage pathways and recombination of charges in the bulk or at the interfaces [12]. The value of R_s and R_{sh} could also be abstracted from the current density–voltage (J–V) curve under illumination.

The PCE (η) is calculated using the equation

$$\eta = \frac{V_{oc} I_{sc} \mathrm{FF}}{P_{light}} \tag{1}$$

where P_{light} is incident light power, FF is calculated by the following formula:

$$\mathrm{FF} = \frac{V_{max} I_{max}}{V_{oc} I_{sc}} \tag{2}$$

The curvature of the J–V characteristics in the fourth quadrant can vary from convex (FF > 50%) to concave (FF < 12.5%) depending upon these parameters. The physical meaning of key parameters for solar cells is defined in Fig. 1.

It is generally believed that the difference in potential between the LUMO of acceptor and the HOMO of donor affects V_{oc} when the contact is perfect Ohmic contact (non-injection in the reverse bias mode). This perfect Ohmic contact, however, cannot be achieved in practical cells. And the difference in work function between the electrodes has the major effect on the V_{oc}. Scharber et al. [32] reported that the V_{oc} of a cell based on a blend of donor polymer and $PC_{60}BM$ (chosen as being the best acceptor materials so far) is dictated to the following relation:

$$V_{OC} = \frac{1}{e}\left(\left|E_{HOMO}^{donor}\right| - \left|E_{LUMO}^{acceptor}\right|\right) - 0.3 \tag{3}$$

where e is the elementary charge, and the value of 0.3 V in Eq. (3) is an empirical factor which is related to the coulomb attraction between holes and electron. The energy difference between the LUMOs of donor and acceptor should be larger than 0.3 eV for efficient charge separation, which strongly determines the J_{sc} of cells [32,33]. The PCE of a BHJ solar cell should be more sensitive to the changes of donor LUMO level compared to the variation of donor bandgap, as shown in Fig. 2.

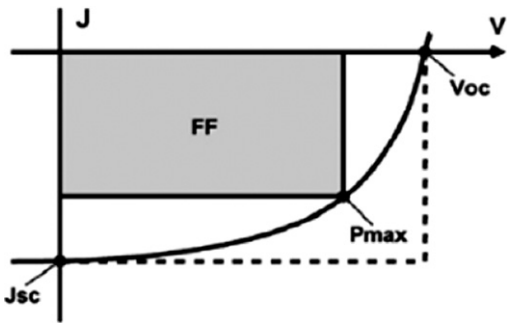

Fig. 1. J–V curve for a typical solar cell. Geometrically, the fill factor (FF) can be visualized as the area ratio of the gray rectangle and the dashed rectangle ($P_{max}/V_{oc}J_{sc}$).

3. Typical materials

3.1. Small molecular materials

Generally, organic semiconductors have low dielectric constant ($\varepsilon \approx 3$) and high absorption coefficient of ($>10^5\,cm^{-1}$), which means that thin layer can still be highly absorptive while simultaneously preserving good charge transport performance. Organic semiconductor could be classified as small molecule and polymer according to its molecular weight, or electron donor and electron acceptor according to its electron gaining and loss ability. When a photon was absorbed by an electron donor, the electron was excited to an excited energy state which binds with the holes to form exciton with a binding energy of about 0.3–0.4 eV. The exciton will diffuse to the interfaces between electron donor and electron acceptor under the built-in electric field and be dissociated into free charge carriers. Charge carriers induced by exciton dissociation will be collected by their corresponding electrodes, respectively.

The common used small molecular electron donor materials are pentacene [34], tetracene [35] and different metal phthalocyanines (MePc) [36,37]. For electron acceptor materials, perylene compounds like 3,4,9,10-perylenetetracarboxylic bis-benzimidazole (PTCBI) [38,39] and C_{60}, C_{70} [40–42] are commonly used in small molecular solar cells. An important characteristic of optoelectronic materials is the presence of a direct bandgap, which allows electronic transitions between the LUMO and HOMO to proceed without the intervention of phonons [43]. Different configurations of carbon, for instance carbon nanotubes (CNTs), graphene, graphite, C_{60} and C_{70}, have shown great potential application as electron accepting and transporting materials, as well as transparent electrode. C_{60} has become the most preferred electron-accepting and transporting material for OSCs. Xi et al. reported that the cells using C_{70} as electron acceptor show higher J_{sc}, V_{oc}, FF, and PCE than those using C_{60} as electron acceptor with the same donor material, because of its higher responsibility in visible region and better electron transport and quantum current distribution in C_{70} molecule [44]. For the cells with C_{60} as electron acceptor, more carriers and excitons will be recombined in C_{60}-acceptor, and cause a lower J_{sc} of the cell. The most popular soluble electron acceptor materials are [6,6]-phenyl-C-61-butyric acid methyl ester ($PC_{60}BM$) and [6,6]-phenyl-C-71-butyric acid methyl ester ($PC_{70}BM$) [45,46], while the $PC_{60}BM$ has a weak absorption in visible light region and a low LUMO energy level. Although a series of C_{60}, C_{70} derivatives and a new C_{84} derivative have been synthesized and used as an acceptor in OSCs [47–50], most of them show the poorer or similar behavior with PCBM. Therefore, it is very important to design and synthesize new soluble fullerene derivatives with stronger visible absorption and higher LUMO energy levels than PCBM. In 2009, Ross et al. [51] reported a novel endohedral fullerene, $Lu_3N@C_{80}$-PCBM, possesses a higher LUMO energy level than $PC_{60}BM$. The P3HT-based polymer solar cell (PSCs) with $Lu_3N@C_{80}$-PCBM as acceptor showed a 260 mV higher V_{oc} than the reference devices with $PC_{60}BM$ as acceptor. However, the high cost of $PC_{70}BM$ and $Lu_3N@C_{80}$-PCBM will limit their future commercial application in OSCs. Recently, He et al. [52] reported a new soluble C_{60} derivative, indene-C_{60} bisadduct (ICBA), with a LUMO energy level 0.17 eV higher than that of PCBM. The PSCs based on P3HT with ICBA as acceptor show a higher V_{oc} of 0.84 V and higher PCE of 5.44% under the illumination of 100 mW/cm^2, with OSCs based on P3HT/PCBM displaying a V_{oc} of 0.58 V and PCE of 3.88% under the same experimental conditions. It means that the ICBA may become an alternative high performance acceptor and be widely used in PSCs. The chemical structures of the typical small molecular materials are depicted in Fig. 3.

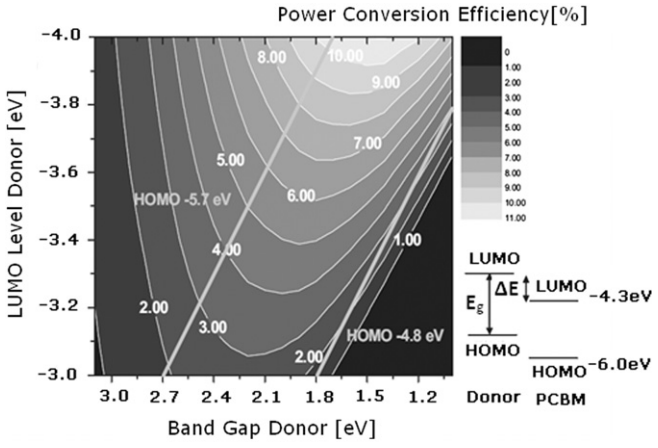

Fig. 2. Contour plot showing the calculated energy-conversion efficiency (contour lines and colors) versus the bandgap and the LUMO level of the donor polymer according to the model described above. Straight lines starting at 2.7 and 1.8 eV indicate HOMO levels of −5.7 and −4.8 eV, respectively. A schematic energy diagram of a donor PCBM system with the band gap energy (E_g) and the energy difference are also shown [32].
Copyright Wiley-VCH Verlag GmbH & Co. KGaA. Reproduced with permission [32].

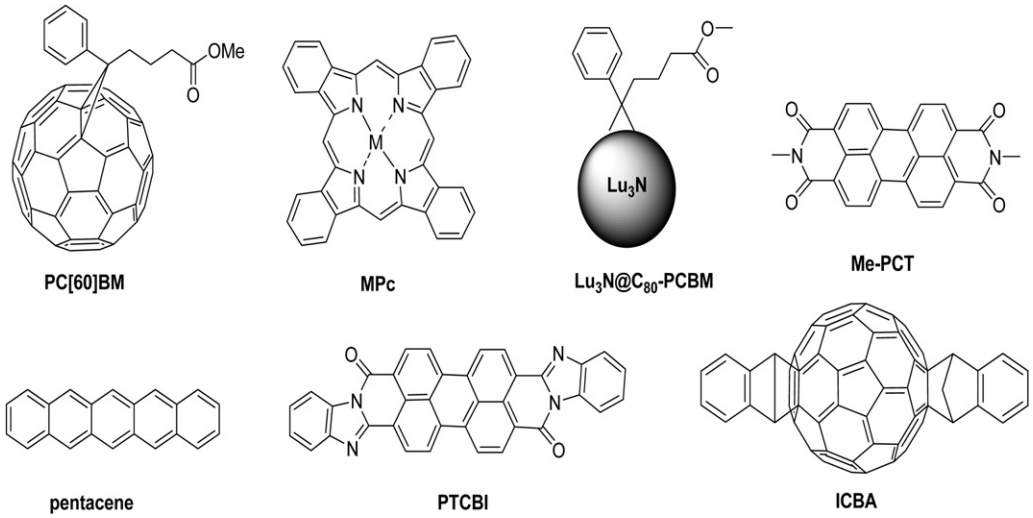

Fig. 3. The chemical structure of typical small molecular materials.

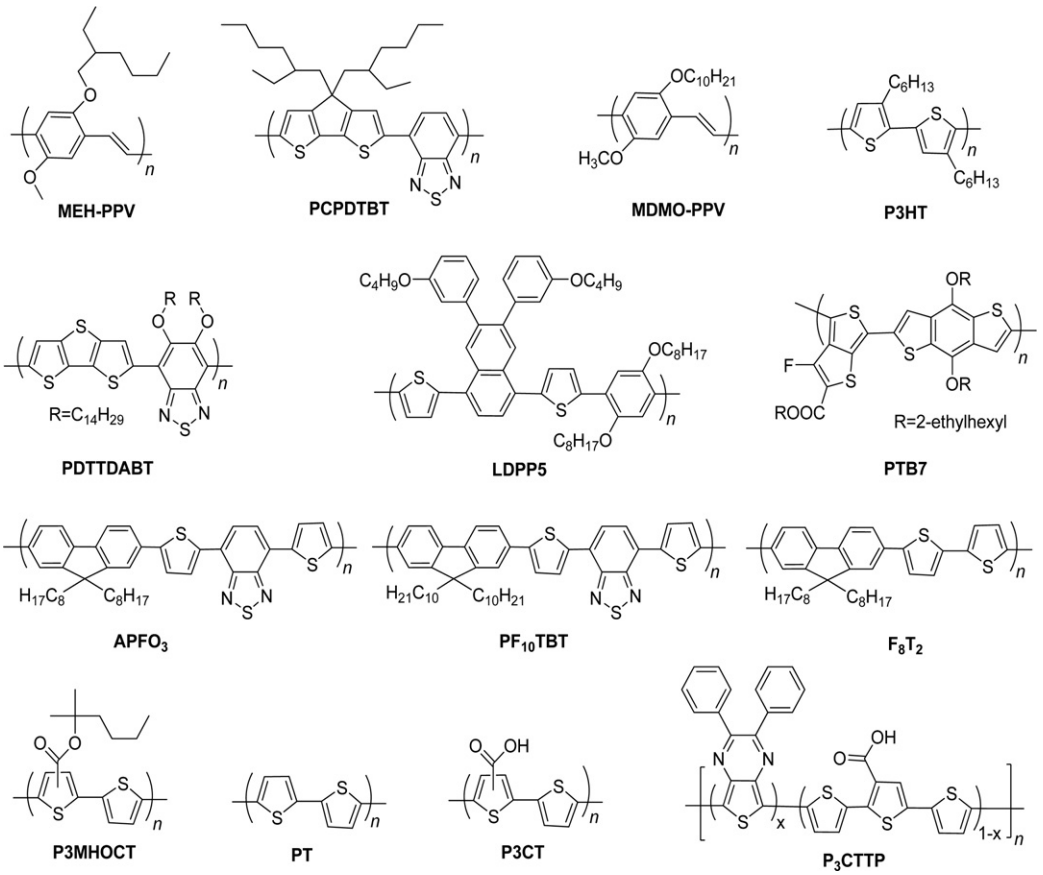

Fig. 4. The chemical structures of typical electron donor polymer.

3.2. Polymer materials

Poly(3-hexylthiophene) is the most representative conjugated polymer donor material. However, its OSCs application is limited by its relatively wide bandgap ~2.0 eV and thus lack broad absorption profile to collect a large fraction of the solar spectrum (ca. ≤30%) [53–55]. Furthermore, a relatively high-lying HOMO energy level determines the maximum cell V_{oc} to 0.60–0.65 V, which a potential trigger of device instability under ambient conditions [55]. To harvest solar energy over a broader spectrum range, it is highly desirable to develop conjugated polymers with broader absorptions through narrowing down their optical bandgap. A large spectrum of low bandgap polymers have been developed over the years to better match the solar spectrum, especially in the 1.4–1.9 eV region. The chemical structures of typical high efficient donor materials are summarized in Fig. 4.

As shown in Fig. 4, a powerful strategy in designing low bandgap conjugated polymers is to alternate a conjugated electron-rich donor (D) unit and a conjugated electron-deficient acceptor (A) unit in the same polymer backbone. With the alternation of D–A units, the bandgap of the polymer can be effectively reduced [56]. The magnitude of the bandgap and the alignment of the HOMO and LUMO energy levels are the most important characteristics in determining the optical and electrical properties of a given conjugated polymer. These also greatly affect the ultimate photovoltaic performance of resultant PSCs. The most straightforward way to reduce the bandgap can be simple by either raising the HOMO or lowering the LUMO level of the polymer or by compressing the two levels closer together simultaneously. However, donor's energy level manipulation is only one consideration in bandgap engineering. The energy level of acceptor material should also be taken into account for higher PCE. According to Eq. (3), V_{oc} is determined by the energy level difference between the HOMO of electron donor and the LUMO of electron acceptor. Therefore, the lower HOMO energy level of electron donor, the higher V_{oc} can be achieved. And narrowing down polymer's bandgap by lifting up its HOMO level will inevitably result in a loss of V_{oc}. On the other hand, the LUMO energy level of donor materials has to be at least 0.3 eV higher than that level of the fullerene derivatives to guarantee the formation of a downhill driving force for the charge carriers separation and transfer [57,58]. In this case, narrowing down polymer's bandgap by pushing down its LUMO level will inevitably lead to a loss of J_{sc}, which is related to the charge carrier transfer and the absorption in the visible light range. As a whole, it is challenging to obtain high J_{sc} and V_{oc} simultaneously. In typical narrow bandgap polymers, D units generally adopt fluorene, carbazole, thiophene and their derivatives, while A units use 2,1,3-benzothiadiazole and other electron-withdrawing building blocks. To achieve high PCE in polymer BHJ cells, one should take into account all issues including material structures, absorption wavelengths, bandgap, charge carrier mobility, and the phase separation between electron donors and electron acceptors. The more detailed information about conjugated oligomers for high-efficiency bulk-heterojunction solar cells can be found in our previous review [59].

4. Recent development of inverted configuration OSCs

4.1. Inverted configuration small molecular OSCs

The commonly used organic small molecular materials are metal phthalocyanine and C_{60} as electron donor and electron

acceptor, respectively. In a conventional small molecule OSCs, a buffer layer, such as bathocuproine (BCP), bathophenanthroline (Bphen), 1,3,5-tris(2-N-phenylbenzimidizolyl) benzene (TPBi), and tris-8-hydroxy-quinolinato aluminum (Alq_3), is inserted between the acceptor and the cathode to prevent exciton quenching [60–63]. So far inverted small molecule solar cells have only a few reports [64,65]. Tong et al. [64] reported an inverted configuration small molecular OSCs based on subphthalocyanine (SubPc)/C_{60} planar heterojunctions. The inverted configuration cells achieved a PCE of $2.4 \pm 0.2\%$, or approximately 75% that of a conventional planar SubPc/C_{60} cells on ITO substrates (with a power efficiency of $3.3 \pm 0.1\%$). The V_{oc} of the inverted configuration OSCs, optimized by tailoring the work function of the layers adjacent to the donor and acceptor, is comparable to the normal configuration cell's V_{oc} 1.10 ± 0.02 V. In our pervious works, we also reported a kind of inverted configuration OSCs with Ca modified ITO as the electrode and MoO_3 modified Ag as the anode [65]. The *J–V* characteristic curves of the inverted configuration OSCs under 100 mW/cm^2 are shown in Fig. 5. It is distinguished that the cell efficiency is remarkably enhanced by the introduction of 1 nm Ca layer. The V_{oc}'s of 0.35 and 0.39 V for both inverted configuration OSCs with 0 and 1 nm Ca are quite close, similar to that of a normal cell. The V_{oc} is significantly correlated with the insertion of ultrathin Ca layer due to the energetic competition of charge collection between ITO/Ca/PCBM and ITO/Ca/P3HT [66–68]. Herein, the resultant V_{oc} indicates that the Fermi level pinning can be formed at either ITO/C_{60} interface or ITO/Ca/C_{60} interface. This has also been proved that C_{60} as a self-assembled monolayer (SAM) inserted between TiO_2 and polymer blend layer functions as multiple roles for increasing the photocurrent and FF in inverted BHJ OSCs [69]. Due to the unique properties of C_{60}, an ultrathin C_{60} interlayer was used to modify the work function of metal and to reduce charge injection barrier between metal and organic layers [70,71]. The quasi-Ohmic contact could be formed at interfaces between high work function metals and C_{60} layer [70]. On the other hand, an ultrathin C_{60} interlayer lowers the work function of ITO and also makes it work as cathode, similar to that in inverted configuration PSCs. Therefore, this insertion of Ca layer facilitates electron collection and blocks hole collection, leading to the improved charge selectivity and the reduced leakage current. Both inverted

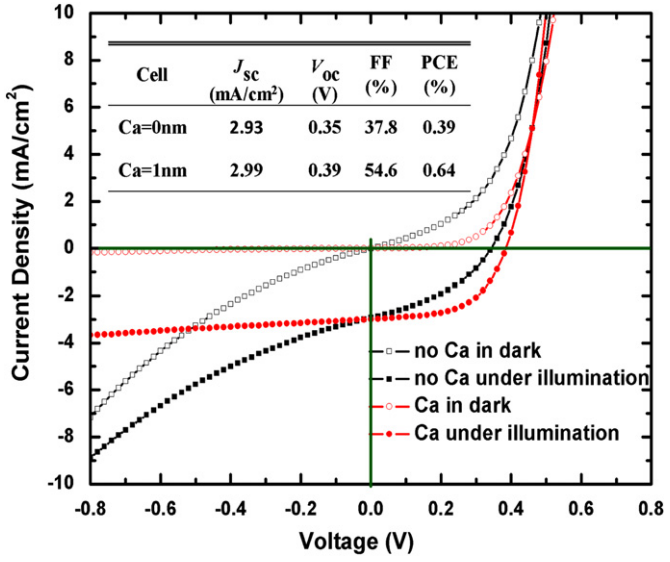

Fig. 5. The *J–V* characteristics of the inverted cells with bare ITO substrates and with 1 nm Ca modified ITO substrate in dark and under illumination. Adapted permission from [64]. Copyright 2010 Elsevier.

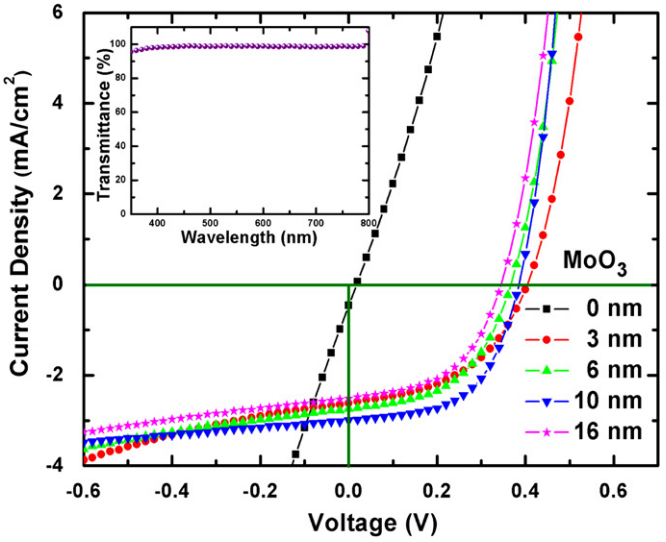

Fig. 6. The *J–V* characteristics of the inverted cells with 1 nm Ca modified ITO substrate and different MoO_3 thickness under 100 mW/cm^2. The inset shows the transmittance spectrum of 16 nm thick MoO_3. Adapted permission from [64]. Copyright 2010 Elsevier.

configuration OSCs show the similar current density 2.93 and 2.99 mA/cm^2. In contrast, in the inverted configuration OSCs, the contamination to C_{60} originating from metal deposition is prevented, thus, it is not necessary to insert a protection layer between C_{60} and ITO. This is likely another reason for the close photocurrents obtained.

A buffer layer used for modifying anode plays an important role in the device performance, which should possess good hole-transporting capability, high transparency, and matched energy levels between active layer and anode. The *J–V* characteristics of these inverted cells under 100 mW/cm^2 are shown in Fig. 6.

With the insertion of MoO_3 layer, the performance of inverted configuration OSCs was remarkably boosted. This can be explained by the following three aspects: (i) the MoO_3 energy levels making it act as an exciton-blocking layer to prevent exciton quenching near Ag anode due to the larger energy bandgap of MoO_3 (around 3 eV) [68]; (ii) ineffective collection of holes by Ag anode due to large mismatch between the work function of Ag and the HOMO of CuPc [72]; (iii) the protection of CuPc layer from being damaged by Ag metal deposition. In addition, the V_{oc} of inverted configuration OSCs slightly decreases when the MoO_3 thickness increases, primarily due to the increase of voltage loss across relatively thick MoO_3 layer.

The performance of inverted configuration OSCs ITO/Ca/C_{60}/CuPc/MoO_3/Ag is closely correlated with the thickness of absorption layer and interface contact. 1 nm Ca layer inserted between ITO and C_{60} largely enhances the FF and overall efficiency. MoO_3 interlayer could effectively improve the interfacial contact between CuPc and Ag anode, resulting in the distinguished improvement of FF due to the increase of shunt resistance and the decrease of series resistance. Upon the optimized thickness of each layer, the maximum PCE of 0.64% was obtained under 100 mW/cm^2 illumination for the inverted configuration cells based on 1 nm Ca modified ITO as cathode, 25 nm thick CuPc layer as absorption layer, and 10 nm MoO_3 modified Ag as anode.

4.2. Inverted configuration bulk heterojunction OSCs

Semiconducting polymers are appropriate materials for developing low-cost technologies for large-area solar cells, because polymers can be deposited from solution using simple methods

such as spin-coating and ink-jet printing [73,74]. Inverted configuration OSCs with polymer as the active layers have attracted more and more attention during the recent years [28,64,75–77]. More than one hundred papers about inverted configuration OSCs have been published in 2009 and 2010. In conventional OSCs, it has been found that P3HT:PCBM based bulk heterojunction active layer exhibits a vertical phase separation, i.e. PCBM-rich at the bottom (closer to ITO side) to P3HT-rich atop (farther away from the ITO) [78–80], therefore, both charge transport and charge collection are obstructed in the conventional structure OSCs. To improve the interface stability and charge transport/collection, an alternative approach is to adopt inverted configuration [81,82], where ITO serves as the cathode and a high work function (HWF) metal as the anode. It is obvious that only modified ITO by functional layers such as TiO_2[83], ZnO [84–89], and alkali-metal-compound cesium carbonate (Cs_2CO_3) [90,91], can serve as the effective cathode for electron extraction. Generally, TiO_2 and ZnO can be used in the forms of thin film and nanostructure prepared by wet methods, in which nanostructures offer additional heterojunctions at the interfaces of donor polymer and nanostructures for exciton dissociation to produce more photocurrent. On the other hand, Cs_2CO_3 can be prepared by both thermal evaporation and solution process. Liao et al. demonstrated that work function of ITO electrode was decreased from 4.5 to 3.06 eV by spin coating an ultrathin Cs_2CO_3 onto ITO surface [29]. The Cs_2CO_3 layer can be decomposed into low work function cesium oxide by annealing at 150 °C, which is consistent with the fabrication procedures of the active polymer layer. The PCE of inverted OSCs with Cs_2CO_3-modified ITO cathode reaches 4.2% after annealing treatments, which is comparable to the regular structure device on the same system. However, Cs_2CO_3 is very sensitive to moisture and thus Cs_2CO_3 modified ITO cathode can be easily degraded due to air-leakage through the edges of the encapsulation. These interfacial layers are designed to achieve the energy level alignment between electrodes and adjunct active layers (donor and acceptor), aiming to minimize the Ohmic loss during charge transfer. Recently, Sun et al. [92] reported that P3HT nanofibers can be synthesized by utilizing its interaction with marginal solvents, which offer the possibility of directed charge transport and improved absorption due to better chains ordering.

Recently, Kyaw et al. reported an efficiency of 3.09% inverted configuration BHJ P3HT:PCBM solar cell with a highly transparent sol–gel derived ZnO film as electron selective layer and MoO_3 as hole selective layer [93]. By modifying the precursor concentration of sol from 0.75 to 0.1 M, the optical transmittance of ZnO film increases from 75% to 95%. This improvement in transmittance increases the J_{sc} of inverted configuration OSCs from 5.986 to 8.858 mA/cm^2 without sacrificing the V_{oc} and FF of the device. It is demonstrated that the device incorporated with MoO_3 has a larger V_{oc} and FF in comparison to the device without MoO_3. Chou et al. introduced a solution-processed vanadium oxide (V_2O_5) between organic layer and the Ag electrode as an anode interlayer to improve the performance of the low-cost inverted configuration OSCs hybridized with ZnO nanorods [94]. The PCE of the inverted configuration OSCs was improved from 2.5% to 3.56% with the introduction of V_2O_5 interlayer. The V_2O_5 interlayer also serves as an optical spacer to enhance light absorption, and thereby increases the photocurrent. Solution-processed V_2O_5 as an anode interlayer without annealing has been reported, the PCE of inverted configuration cells made with V_2O_5 modified ITO anode was shown to increase from 2.5% to 3.56% compared to the similar cells without the V_2O_5 interlayer [11]. Compared to vacuum-deposited techniques, fabrication of solution-processed V_2O_5 interlayer is simpler and more effective. This solution-processed V_2O_5 is relatively insensitive to moisture and oxygen and advantageous in non-annealing treatment. The solution-based approach makes it attractive for applications in mass production and potentially printed organic electronics. A BHJ OSCs usually consists of a large area of donor/acceptor interfaces for charge separation at the expense of discontinuous transport pathways through hopping. Alternatively, OSC structure consisting of direct and ordered paths for photogenerated carriers to the collecting electrodes has been proposed. Lin et al. also demonstrated an improvement of photovoltaic performance based on the nanostructured ZnO/P3HT hybrid through interface molecular modification on ZnO nanorod surface [94]. By probing the carrier dynamics at ZnO/P3HT interfaces, it was found that the interfacial molecules can play the role of assisting charge separation and suppression of back recombination at interfaces, which accounts for the observed enhanced J_{sc} (from 0.3 to 2.45 mA/cm^2) and V_{oc} (from 0.34 to 0.46 V) in OSCs. Recently, Menon et al. investigated that the role of In_2S_3 as a potential electron selective layer in PSCs could effectively increase the PCE of inverted configuration PSCs compared to the similar cells without electron selective layer [95]. Up to now, organic molecule of mercurochrome [$C_{20}H_8Br_2HgNa_2O$] has been found as one of the best photosensitizers for ZnO photoanode. Zhao et al. obtained a high efficiency inverted configuration OSCs, consisting of an ultrathin Ca layer for electron transport, the blend of P3HT:PCBM for photon absorption, and a MoO_3 layer for hole transport [96]. The insertion of MoO_3 layer between photoactive layer and Ag anode has been demonstrated to improve both the photocurrent and FF. By optical modeling and experiment, it is found that the MoO_3 layer also functions as an optical spacer for these kinds of OSCs. The maximum PCE of 3.86% was achieved in the optimized device with an active layer thickness of 85 nm, Ca thickness of 0.5 nm, and MoO_3 layer thickness of 5 nm. Baek et al. reported that a hybrid inverted bulk heterojunction OSCs with nanoimprinted TiO_2 nanopores showed higher PCE of 1.49% than on flat TiO_2 (PCE$\sim$1.18%) [97]. Huang et al. investigated the effect of interface quality between organic and inorganic nanostructures on the performance of organic–inorganic hybrid device based on polymer/fullerene blend and ZnO nanorod array [73]. A fullerene interlayer was spin-coated onto the ZnO nanorod surface to modify ZnO nanorod interface. The PCE of modified inverted configuration OSCs was improved from 2.35% to 3.2%, with a J_{sc} of 11.67 mA/cm^2, an V_{oc} of 0.55 V, and a FF of 0.5 under 100 mW/cm^2 irradiation. This improvement could be reasonably explained by the enhanced optical absorption because this fullerene interlayer helps the polymer to self-organize and improves the infiltration of the photoactive layer into ZnO nanorod spacing. Rider et al. reported that the synthesis of a cationic and water-soluble polythiophene [poly[3-(6-pyridiniumylhexyl)thiophene bromide] (P3PHT$^+$Br$^-$)] was synthesized and its application in the combination with PEDOT:PSS to produce hybrid coatings on ITO substrates [75]. The coatings are found to modify the work function of ITO such that it could act as an effective cathode in inverted configuration OSCs based on P3HT:PCBM blend as the active layer. The interfacial modifier created from the layer-by-layer assembly route was used to produce efficient inverted configuration OSCs (PCE 2%) with significant long-term stability in excess of 500 h. The water-soluble polymers are particularly advantageous as organic solvents are relatively expensive and environmentally harmful. In order to present an insight view about inverted configuration OSCs, some typical inverted configuration OSCs schematic diagrams are summarized in Fig. 7. The detailed cell structure and photovoltaic characteristics of representative inverted configuration OSCs in recent years are summarized in Table 1.

It is worthwhile to mention that a novel PCBM-based n-type material, [6,6]-phenyl-C61-butyric styryl dendron ester (PCBSD), functionalized with a dendron containing two styryl groups as thermal cross-linkers, has been rationally designed and easily synthesized [30]. Inverted OSC with a configuration of ITO/ZnO/PCBSD/P3HT:PCBM/PEDOT:PSS/Ag achieves an impressive PCE of 4.4% and exceptional device lifetime without encapsulation. This

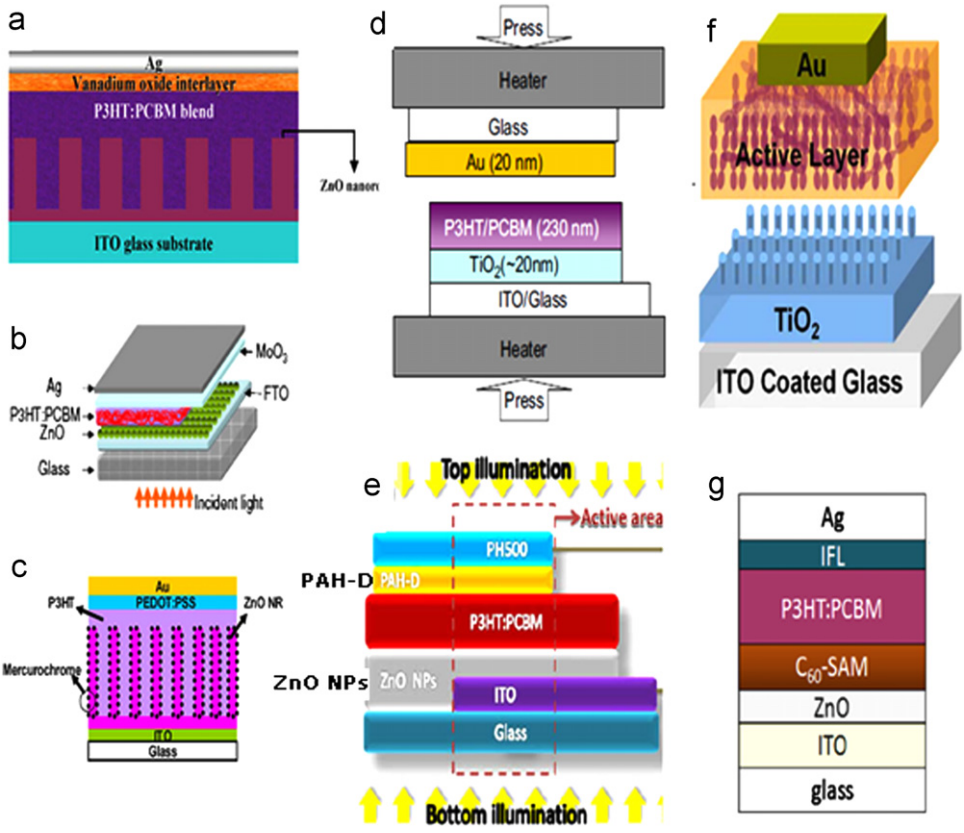

Fig. 7. the summary of typical inverted OSCs schematic diagrams [92,95–99,76].

Table 1
The key parameters of some typical inverted OSCs with different electrodes interlayer.

Cell ID	Structure			J_{sc} (mA/cm^2)	V_{oc} (V)	F.F. (%)	PCE (%)	Ref.	Year
	Anode layers	Active layers	Cathode layers						
1	FTO/ZnO	P3HT:PCBM	MoO_3/Ag	8.858	0.616	57	3.09	[85]	2008
2	ITO/ZnO	P3CT:ZnO	PEDOT:PSS/Ag	0.91	0.49	29.6	0.13	[93]	2008
3	ITO/ZnO	P3CTTP:ZnO	PEDOT:PSS/Ag	0.28	0.25	31.1	0.02	[93]	2008
4	ITO/ZnO	P3CT:ZnO P3CTTP:ZnO (tandem)	PEDOT:PSS/Ag	0.15	0.54	25.8	0.02	[93]	2008
5	ITO/ZnO	P3HT:PCBM	V_2O_5/Ag	10.75	0.55	60.2	3.56	[94]	2009
6	ITO/ZnO (NR)	P3HT	PEDOT:PSS/Ag	2.45	0.46	46	0.52	[94]	2009
7	ITO/ZnO	P3HT:PCBM	Ag	11.7	0.53	58	3.58	[100]	2009
8	ITO/TiO_2	P3HT:PCBM	ITO (top)	7.8	0.51	54	2.1	[101]	2009
9	ITO/ZnO/PCBM	P3HT:PCBM	Ag	11.67	0.55	50	3.2	[73]	2010
10	ITO/Ca	P3HT:PCBM	MoO_3/Ag	–	–	–	3.86	[67]	2010
11	ITO/ZnO	PDTTDABT:PCBM	PEDOT:PSS/Ag	5.8	0.56	37	1.2	[96]	2011
12	ITO/ZnO	P3HT:PCBM PDTTDABT:PCBM (tandem)	PEDOT:PSS/Ag	3.6	0.82	32	0.94	[96]	2011
13	ITO/TiOx	P3HT:PCBM	PEDOT:PSS/Au	7.84	0.76	63	3.81	[102]	2010
14	ITO/ZnO	P3HT:PCBM	Graphene oxide/Ag	8.7	0.64	64.5	3.61	[77]	2010
15	ITO/ZnO	P3HT:PCBM	PEDOT:PSS/Ag	8.4	0.54	39	1.79	[103]	2010
16	ITO/ZnO	PT:PCBM-analog	PEDOT:PSS/Ag	4.46	0.49	32	0.7	[104]	2011
17	ITO/ZnO	P3HT:PCBM	PEDOT:PSS/Ag	11.17	0.62	54.3	3.78	[81]	2008
18	ITO/WPF-6-oxy-F	P3HT:PCBM	PEDOT:PSS/Ag	8.37	0.6	44	2.23	[105]	2010
19	ITO/ZnO/C-PCBSD	P3HT:PCBM	PEDOT:PSS/Ag	12.8	0.6	58	4.4	[30]	2010
20	ITO-PET/ZnO	P3HT:PC_{70}BM (large area)	PEDOT:PSS/Ag	22.08 mA	8.61	51.4	2.75	[106]	2010
21	ITO-PET/ZnO	P3MHOCT:PCBM (large area)	PEDOT:PSS/Ag	11.99mA	4.55	29.7	0.17	[107]	2010
22	ITO-PET/ZnO	P3CT:PCBM (large area)	PEDOT:PSS/Ag	6.971 mA	1.97	32.3	0.05	[107]	2010
23	ITO-PET/ZnO	PT:PCBM (large area)	PEDOT:PSS/Ag	10 mA	5.6	34.6	0.20	[107]	2010

–: The detailed value not given, the values are in the norml range. From 20 to 23, the OSCs are large area cell marked with the current values instead of current density.

cell greatly outperforms the reference cell (configuration ITO/ZnO/P3HT:PCBM/PEDOT:PSS/Ag) without PCBSD interlayer, which presents a PCE of 3.5%. This promising approach can be applied to another inverted solar cell, ITO/ZnO/CPCBSD/PCPDTBT:PC71BM/PEDOT:PSS/Ag, using PCPDTBT as the p-type low-band-gap conjugated polymer to achieve an improved PCE of 3.4% [30]. Recently,

Jo et al. reported that the fabrication of inverted configuration OSCs with graphene cathodes, which demonstrates the application of graphene films as cathodes in inverted configuration OSCs [105]. Graphene is a promising next generation conducting material with the potential to replace traditional materials ITO in optoelectronic devices. It combines several advantageous characteristics including low sheet resistance, high optical transparency, and excellent mechanical properties [108]. It is demonstrated that the inverted configuration OSCs with work-function-engineering of graphene electrode will foster the fabrication of more advanced OSCs with higher efficiency.

4.3. Inverted tandem configuration OSCs

The two major losses occurring in OSCs are the sub-band-gap transmission and the thermalization of the hot charge carriers. One way to circumvent both effects simultaneously is the built-up of tandem cells. Tandem OSCs comprise a bottom cell and top cell connected by an idea fully transparent intermediate layer in series mode, which was originally developed by Hiramoto et al. [109]. Yakimov and Forrest [110] reported a tandem cell with 2.5% high efficiency, more than double of individual cell based on CuPc/PTCBI. Both donor materials in bottom cell and top cell have different bandgap, which enable the absorption over a broad range of photon energies within the solar emission spectrum. The bandgap of donor material in bottom cell is lower than that of donor material in top cell. Therefore, the tandem cell architecture can therefore improve the light harvesting in the active layer. The V_{oc} of tandem solar cell is increased to the sum of the V_{oc}'s of the individual cells, but the J_{sc} is lower than that of each cell. The operation of tandem cells proceeds as the following: (1) light absorption generates excitons in the top and bottom cells; (2) after excitons dissociation in each cells, the hole in the bottom cell and electrons in the top cell are collected and recombined nearby the intermediate layer. The main challenge to realizing tandem cells is in balancing the photocurrent from each cell as the current in the series-connected subcells is limited by the smallest subcell current [111]. When the same donor material was used in the bottom and top cells, the smaller J_{sc} is attributed to the identical absorption spectra of active layer, so that the top cell absorbs less incident light and thus limits the photocurrent (because the two cells is in series, the current through the multilayer device is determined by the top cell). Moreover, because the intermediate layer is only semitransparent, its additional absorption also reduces the intensity of the light incident on the top cell [1]. Herein, the intermediate layer, connecting the subcells optically and electrically, plays a crucial role in overall device performance. Thus far, quite a few intermediate layers have been reported, such as TiO_2/PEDOT:PSS [112], Ag nanocluster [113], Al/Au/PEDOT:PSS [114], ZnO/PEDOT:PSS [115,116], Al/MoO_3 [117], Al/TiO_2:Cs/PEDOT:PSS [118], and MoO_3/Ag/Al/Ca [119], to improve the charge carrier collection and modify the optical field distribution in the top subcell.

In 2010, Sun et al. [119] reported a high efficiency inverted tandem configuration OSCs, consisting of two BHJ subcells with identical P3HT:PCBM, and an intermediate layer made of ultra-thin multiple metal layers of MoO_3/Ag/Al/Ca. Recently, Krebs et al. reported that a solution-processed inverted configuration OSCs, which exhibit good performance comparable to or better than the normal configuration OSCs [96]. All solution processed inverted tandem OSCs with thermocleavable materials exhibited operational stability in air without any form of encapsulation [86]. The typical device structures of inverted tandem configuration OSCs are shown in Fig. 8.

The J–V characteristics of inverted bottom subcell, top subcell, and tandem cell under 100 mW/cm^2 are shown in Fig. 9. The inverted tandem configuration OSCs shows a PCE of 2.78% with a J_{sc} of 3.81 mA/cm^2, V_{oc} of 1.18 V and a high FF of 61.8% when MoO_3(7.5 nm)/Ag (1 nm)/Al(1 nm)/Ca(3 nm) was acted as the intermediate layers [119]. The V_{oc} (1.18 V) of the inverted tandem solar cell is almost the exact summation of V_{oc} (0.57 and 0.63 V) the top subcell and bottom subcell, which demonstrates no voltage loss

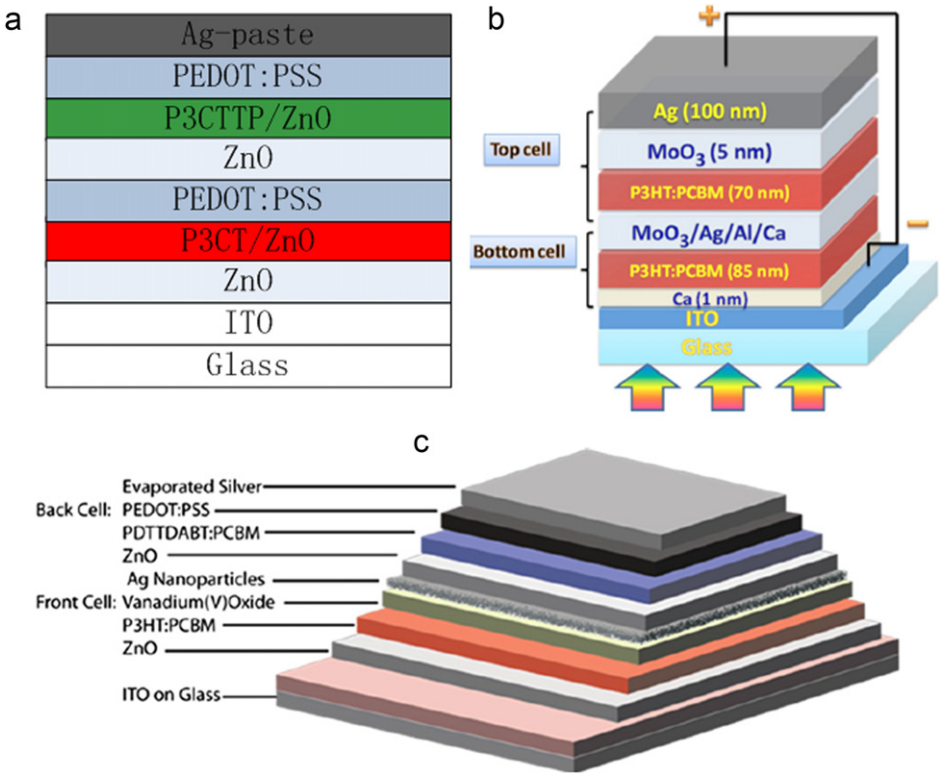

Fig. 8. The summary of typical device structure of the inverted tandem configuration OSCs [93,96,119].

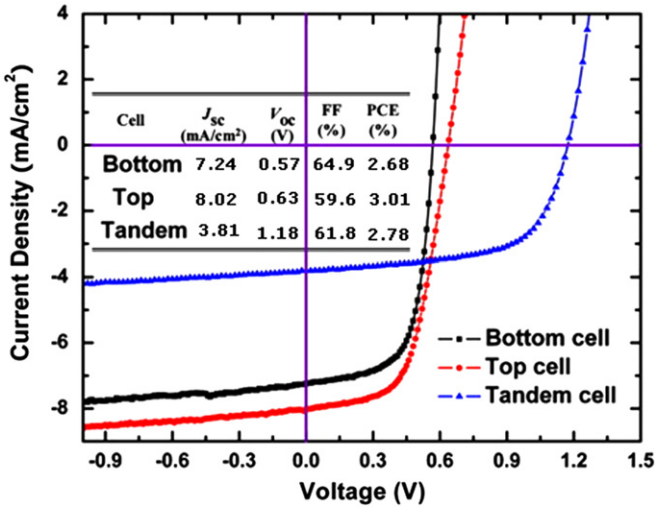

Fig. 9. The *J–V* characteristics of the inverted bottom subcell, top subcell, and tandem cell with MoO_3/Ag/Al/Ca intermediate layer under 100 mW/cm^2. The bottom subcell is with a structure of ITO/Ca(1 nm)/P3HT:PCBM(85 nm)/MoO_3(7.5 nm)/Ag and the top subcell is with a structure of ITO/Ca(3 nm)/P3HT:PCBM(70 nm)/MoO_3(5.0 nm)/Ag. The inset shows the summary of all device performance. Adapted permission from [116]. Copyright 2010 American Physics Institute.

across the intermediate layer. It is highlighted that high FF (61.8%) of the inverted tandem configuration OSCs is comparable to those of normal cells [2], and that of tandem normal configuration OSCs [1].

The working mechanism of inverted tandem configuration OSCs is very similar to that of normal tandem configuration OSCs. The tandem cell architecture is equivalent to two cells in series, offers a number of advantages. The use of two kinds of semiconductor with different bandgaps enables absorption over a broad range of photon energies within the solar emission spectrum. Tandem cells generally use a wide bandgap material as the bottom active layer and a narrow bandgap material as the top active layer, in order to balance the charge carriers at the intermediate layer, the thickness of top and bottom active layers should be optimized. It is generally considered that the thickness of active layer in the bottom cell is thinner than that in the top cell. The V_{oc} of tandem cells should be equal to the sum of V_{oc} of top and bottom subcells because the cells are in series. But the current extracted from the tandem cell is determined by the smaller current generated from top and bottom subcells. It is known that the top cell absorbs the light that is not absorbed by the bottom cell and is illuminated under lower light intensities. Consequently, the top cell produces lower photocurrents. When the same organic semiconductors were used for the top and bottom cells, the small J_{sc} was attributed to the identical absorption spectra, so that the top cell absorbs less incident light and thus limits the photocurrent (because the two cells are in series). Thus, different organic semiconductors with complementary absorption range in the visible light range are generally used in the tandem cells. Accordingly, when there is greater carrier generation in either subcell, these excess charges cannot contribute to the photocurrent and so compensate for the built-in potential across that subcell. This compensation leads to a reduced V_{oc} in the tandem cells. In order to optimize and balance the current in each subcell, Kim et al. tried all possible variations of the normal tandem cell architecture: by changing the order of the active materials, by varying the concentration and ratio of each component in the composite solutions, and by varying the thickness of the two BHJ cell [1]. All these tentative methods are beneficial for the improvement of the inverted configuration OSCs. Inganas et al. [120] reported three major approaches to increase incoupling of light into organic active layer. These methods are plasmon-assisted incoupling, microlenses, and folded reflective solar cells, with structuring on 100 nm level, 10–100 mm level, and 10 mm level. The complexity of the physics goes from advanced to trivial, and the trivial is the most rewarding, as almost doubling of light incoupling can be accomplished. Recently, we also reported the distinguished improvement of PCE achieved in OSCs with 4 nm pentacene interlayer, which was attributed to the effect of nanostructural pentacene interlayer between ITO substrate and polymer layer on the electromagnetic field in polymer layer [121]. Recently, Dennler et al. proposed the design rules for donors in the BHJ normal configuration tandem cell towards 15% PCE [32], which may be applied to inverted tandem configuration OSCs in obtaining both high efficiency and stability cells.

4.4. The stability and degradation mechanism of inverted configuration OSCs

It should be highlighted that high stability of inverted configuration OSCs is inherent when adopting high work function metals as the top electrode. Hau et al. demonstrated that an inverted configuration OSCs possessed much better stability under ambient conditions retaining over 80% of its original conversion efficiency after 40 days while the normal one showed negligible photovoltaic activity after 4 days [81]. These unencapsulated inverted configuration OSCs were stored under ambient conditions and periodically tested for 40 days to gage the cells stability. The normal configuration cells using LiF/Al as the electrode is proved to be very unstable due to its PCE was reduced to less than half of its original value after one day of storage and totally lost after 4 days. The key parameters dependence on the storage time are shown in Fig. 10. The improved stability is attributed to both the PEDOT:PSS layer and Ag electrode. The PEDOT:PSS acts as a barrier preventing oxygen from entering the active layer. In addition, the Ag electrode in air can form a layer of silver oxide which increases its effective work function to -5.0 eV. This matches well with the PEDOT:PSS HOMO of -5.25 eV which improves its electrical coherence at the interface [122]. By having cells stable in air, the encapsulation process can be performed under ambient conditions substantially reducing fabrication complexity leading to cost-effective solar cells. As a note, the cells that were not periodically measured, but only measured at day 0 and day 40 showed no appreciable performance changes which is a good indication that the mechanical degradation of the electrode from multiple measurements are the most likely cause for the decrease in performance.

Jang et al. founded that the PCE of inverted configuration OSCs (ITO/Cs_2CO_3 (0.5 nm)/Active layer (70 nm)/MoO_3 (*x* nm)/Al (100 nm)) is relatively retained even in low temperature while that of normal configuration OSCs (ITO/PEDOT:PSS/Active layer (70 nm)/LiF/Al (100 nm)) rapidly decreased with decreasing temperature and the stability in air is also much better [91]. Fig. 11 shows that the inverted configuration OSCs show better stability than the normal configuration OSCs in ambient air at 295 K for 40 days. The PCE of the inverted configuration OSCs drops to about 93.5% of the initial value, while that of normal configuration OSCs decreases to 87.7%. This may be due to less damage to the ITO in the inverted configuration OSCs because there is no PEDOT:PSS process and the improvement of carrier extraction due to the existence of a thin MoO_3. Fig. 12 shows that the *J–V* characteristics of inverted configuration OSCs and normal configuration OSCs under AM 1.5 illumination at different temperature. While the J_{sc} increases with increasing temperature to 340 K and starts to decrease at temperatures more than 360 K, the V_{oc} decreases gradually with increasing temperature. As a result, the inverted configuration OSCs exhibit their maximum efficiency at $\sim$300 K. The reduction in efficiency of inverted configuration OSCs dependence on temperature is much less as compared to the normal configuration OSCs.

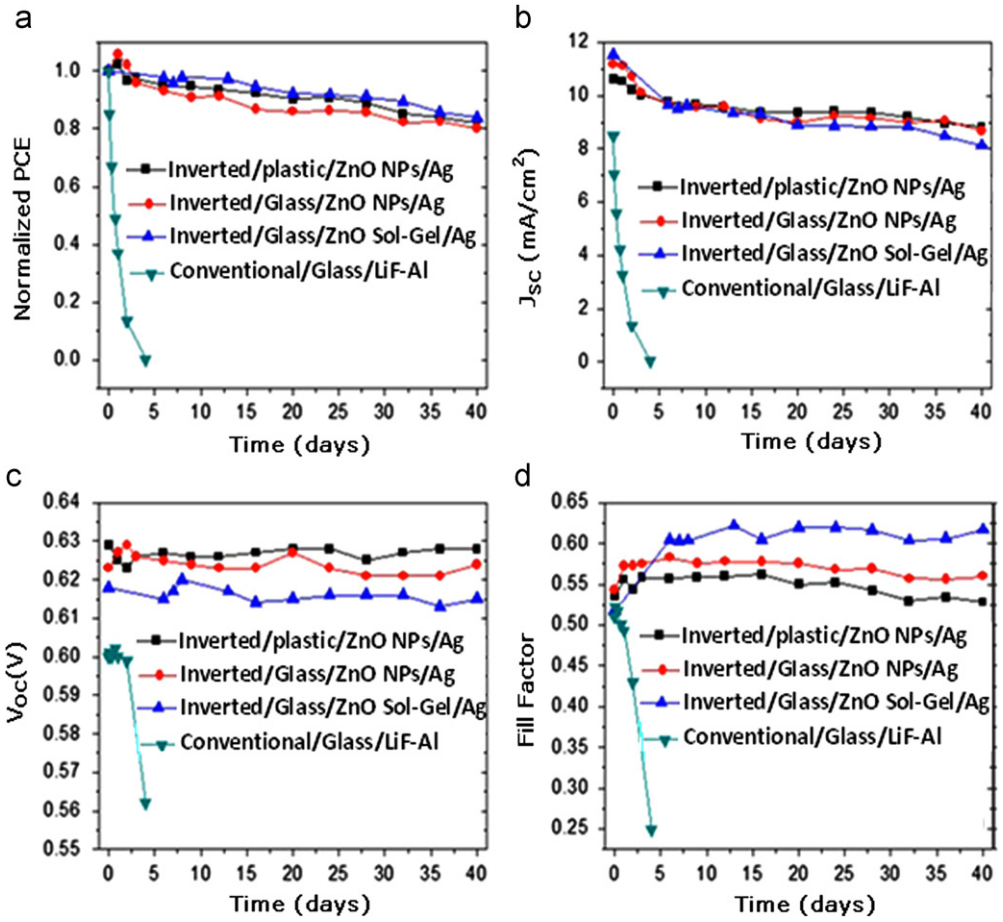

Fig. 10. Device performance of unencapsulated conventional and inverted configuration solar cells stored 40 days in air under ambient conditions: (a) normalized PCE, (b) J_{sc}, (c) V_{oc} and (d) FF. Adapted permission from [80]. Copyright 2011 American Physics Institute.

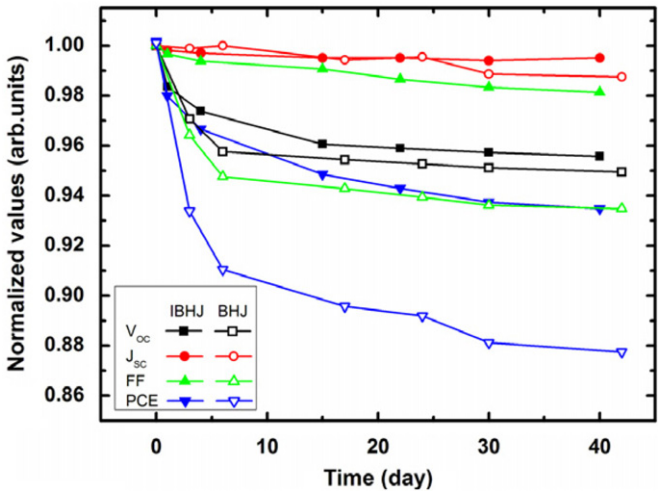

Fig. 11. Plot of solar cell parameters as a function of time in ambient air. The parameters are normalized to initial values. Solid symbols represent the parameters of inverted configuration OSCs and open symbols represent that of normal configuration OSCs. Adapted permission from [91]. Copyright 2011 Elsevier.

Usually, encapsulated OSCs have to withstand certified test procedures such as the damp heat test, an exposure to moist air at 85 °C at 85% relative humidity. The corresponding extrinsic stability, referring to encapsulated devices, is determined mainly by the quality of the encapsulation layers [18]. For an intrinsic lifetime of OSCs, materials and electrodes need to be stable even without any encapsulation. The operational stability has reached thousands of hours under laboratory conditions and up to a year under outside conditions [123,124]. Seemann et al. reported the degradation behavior of an inverted configuration OSCs [125]. They found that due to the gas permeability of the PEDOT:PSS layer, the diffusion of oxygen combined with illumination results in a strong decrease of the J_{sc} within minutes. The J_{sc} could partially be recovered by heating, which was taken as an indicator of degradation occurring in the photoactive layer. Recently, Krebs et al. also studied the degradation patterns of inverted configuration OSCs in water and oxygen [103]. The results indicate the reactions occurring at the interface between active layer and PEDOT:PSS layer were the major cause of device failure in the case of inverted configuration OSCs. Time of flight secondary ion mass spectrometry (TOF-SIMS) depth profiling revealed that $H_2^{18}O$ and $^{18}O_2$ both reacted with the P3HT:PCBM layer and accumulated at P3HT:PCBM/ZnO interface. The reactivity of $^{18}O_2$ toward P3HT:PCBM was approximately twice that of $H_2^{18}O$ under the same conditions. Fig. 13 also shows the result of an experiment where two partial devices (ITO–ZnO–P3HT:PCBM–PEDOT:PSS) were illuminated without encapsulation for 3 weeks in a dry $^{18}O_2$:N_2 or an oxygen free H_2 ^{18}O:N_2 atmosphere (Fig. 13a–d) or in a $H_2^{18}O$ atmosphere (Fig. 13e–h) [103]. The TOF-SIMS images of the PEDOT:PSS surfaces reveal that the layers have phase separated into a PEDOT-rich and a PSS-rich phase. Fig. 13b shows that $^{18}O_2$ reacted almost exclusively with PEDOT, and Fig. 13c reveals that it is at least the sulfur in PEDOT that significantly reacted with $^{18}O_2$. Fig. 13a shows the in-plane distribution of ^{16}O that originates primarily from the $-SO_3H$ group in PSS. Fig. 13e–h shows the corresponding

images for the partial device that was exposed to a $H_2^{18}O$ atmosphere. The phase separation is not as clear, but still visible. $H_2^{18}O$ appears to react to a much lesser extent and not mainly with one phase.

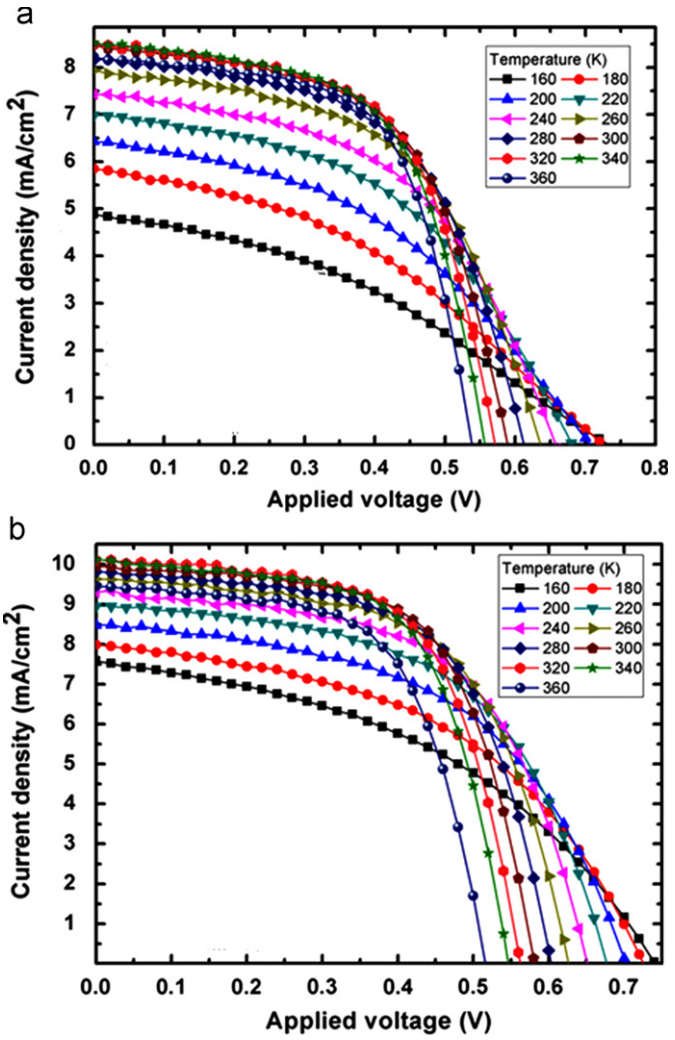

Fig. 12. The *J–V* characteristics of the normal (a) and inverted (b) configuration OSCs under AM 1.5 illumination at low temperatures. The inset shows the extraction of activation energy ΔE and J_0 under illumination. Adapted permission from [91]. Copyright 2011 Elsevier.

The phase separation is more pronounced when a dry $^{18}O_2$:N_2 atmosphere is used as compared to an oxygen free $H_2^{18}O$:N_2 atmosphere. Because phase separation is observed for both atmospheres, it is likely a heat-induced phenomenon possibly affected to some extent by the atmosphere.

Not all degradation processes take place continuously to the same extent and at the same time, a specific degradation process can be restricted to a time window, i.e., a photon dose window. It was also demonstrated that water could diffuse into the cells through the aluminum electrode regardless of whether it is illuminated or not [126,17]. Water appears to be incorporated more efficiently in aluminum oxide in comparison to molecular oxygen. The other prominent degradation pathway was found to be the diffusion of electrode materials into cells. Both electrode materials can diffuse through the entire device to the counter electrode [124]. Under illumination of organic materials, degradation is inevitable albeit slower under inert conditions. The materials degrade and, as a consequence, so do in many instance their physical, electrical, and mechanical properties. The OSCs rely on the delicate interplay between the electronic structure of the material and the energy levels in external electrodes connecting the functional material in the device to the outside world are highly sensitive to even small degrees of degradation. Light absorption and charge-carrier transport properties take place throughout the bulk of the material and at the interfaces. All the processes that are affected by these reaction products in the bulk and at the interfaces will thus lead to degradation of the device performance.

5. Recent progress in potential application

Although vacuum deposition is used industrially in packaging industry and OLEDs fabrication, the vacuum steps lead to a low processing speed, thus limiting the space in production cost cutting. Recently, Zou et al. reported the fabrication of inverted structured PSCs using metal grid/conducting polymer hybrid transparent electrode to replace ITO [127]. The performance of the devices could be easily tuned by varying the width and interval of the metal grids. For the narrowly intervened Ag grids, the addition of the conducting PEDOT:PSS polymer layer can improve the performance of inverted OSCs to 3.21% due to the reduced lateral resistance. The use of inexpensive Ag grids compared to ITO opens the possibility of employing roll-to-roll process for mass production of low cost, large area, and high stability inverted OSCs. Park et al. evaluated the

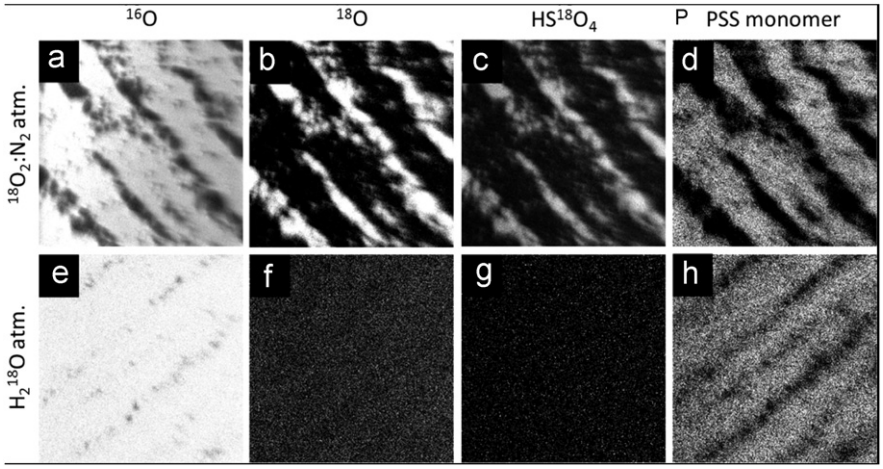

Fig. 13. TOF-SIMS ion images ($500 \times 500\ \mu m^2$) of PEDOT:PSS surfaces from partial devices with the composition ITO-ZnO-P3HT:PCBM-PEDOT: PSS (no Ag electrode). The devices were illuminated (AM1.5, 330 W m^{-2}, 65 ± 2 °C) without encapsulation for 3 weeks in a dry $^{18}O_2$:N_2 (1 atm) atmosphere (A–D) or in an oxygen free $H_2^{18}O$:N_2 ($65 \pm 2\%$ rh) atmosphere (E–H). Black corresponds to 0% signal, gray to some signal, and white to 100% signal. Adapted permission from [103]. Copyright 2010, American Chemical Society.

possibility of utilizing a spray-coating process for large-area OSCs (12.25 cm^2), combined with metal electrode geometry [128]. The series resistance could be reduced significantly by inserting a metal grid electrode into ITO anode, yielding a PCE of 2.11% at a cell area of 12.25 cm^2 and 2.49% at an effective photocurrent generated area of 11.23 cm^2 under AM1.5 simulated illumination. This is comparable to 3.13% PCE obtained in the cell fabricated by spray-coating at a cell area of 0.38 cm^2. Using roll-to-roll techniques, materials can be deposited onto a flexible substrate from liquid phase by printing [106,107,129–131]. Krebs et al. has reported a series of landmark research works in the development of large area, high stability, high efficiency, and different configuration PSCs [103–107,123,124,126, 129–133]. Recently, Krebs et al. reported a technique that enables the probing of the entire parameter space for each parameter with good statistics through a simple roll-to-roll processing method where gradients of donor, acceptor, and solvent are applied by differentially pumped solt-die coating [132]. The first large area solar panels fabricated from PSCs and connected to the grid was recently reported [133]. It was found that the choice of layer structure used to encapsulate the flexible polymer solar modules is the most critical parameter in preserving performance upon panel fabrication, and also plays a key role in panel stability. The best panel reached a maximum peak power of 8 W, and the final set of panels retained 80% performance over 1 month. Panels were connected to the grid between testing, and generated a total of >3 kWh during the study. A cost analysis revealed that the cost of power produced by polymer solar panels is currently more than one order of magnitude above the price of energy produced by silicon panels. The cost of incorporating the polymer cells into a rigid protective panel is found to be a major contribution to the total cost, implying that it is most beneficial to pursue strategies and applications where PSCs are not used in traditional large-area panels. Galagan et al. developed an alternative ITO-free transparent anode, based on solution-processed high conductive PEDOT:PSS in combination with a printed current collecting grid [134]. The screen-printed silver grid demonstrates a typical sheet resistance of 1 $\Omega/\square$ with 6.4–8% surface coverage. The efficiency of a flexible device with an active area of 4 cm^2 with such a grid is much higher than a similar device based on ITO. Furthermore, since this composite anode is solution-processed and free from the rather expensive vacuum-deposited ITO, it is a step forward towards low-cost large area processing. The scale up from laboratory to process scale is not trivial because the morphology and efficiency of the films depends strongly on the processing conditions. By focusing development on the large areas processing techniques, it may be possible to provide a place for polymer solar technology in applications such as off-grid generation in remote and developing locations [135], where their light weight and mechanical durability/flexibility overweight their low stability and large area required.

Recently, the National Energy Renewable Laboratory (NREL) certified that Konarka's OSCs demonstrated a world-record breaking efficiency 8.3%, the highest performance recorded by NREL for OSCs [136]. Konarka Company also developed long lifetime encapsulated OSCs, which were able to maintain a high performance on rooftop for almost 2 years. Solarmer Energy, Inc. also has reported another world record 8.13% efficiency of OSCs [137]. Heliatek GmbH and the institute of applied phtotophysics at Dresden University have reported 8.3% efficiency for an active area of 1.1 cm^2, which was measured by Heliatek and independently confirmed by the Fraunhofer ISE CalLab [138].

6. Conclusion

The current performance of OSCs technology is limited (as compared to silicon-based solar cells) by mainly two factors: (i) the efficiency, which is on the order of 5% (although a few reports of efficiencies approaching higher values in the 6–8% range have appeared recently) [136–138], and (ii) the lifetime, which is on the order of years under outdoor conditions with good stability being recorded for both air stable devices and encapsulated devices [123,124]. The inverted configuration OSCs is the appealing alternative to the conventional regular structure due to the inherent vertical phase separation, improved stability, and flexibility in designing tandem OSCs. Therefore, the advantage of the inverted structure in polymer morphology evolution is naturally identified. Manipulation of film morphology via vertical phase separation and utilization of the inverted structure allow us to derive a normal structure-design rule for OSCs in the potential application. In principle, the strategies used to improve the normal and inverted configuration OSCs efficiency include (i) reducing the bandgap of polymers so as to harvest more sunlight, which leads to higher J_{sc}, (ii) lowering HOMO of the donor polymers, which results in higher V_{oc} and, (iii) using the tandem cell structures. Morphology control crucially remains the key issue to achieve high performance for OSCs. An ideal morphology consists of nanoscale phase separation, with an interpenetrating network of the two separate phases for efficient exciton dissociation. It is very imperative to obtain a bicontinuous network with a domain width approximately twice that of the exciton diffusion length and high donor/acceptor interfaces, which favor the exciton dissociation and transport of the separated charges to the corresponding electrodes. Many researches on interfacial modification at the interfaces nearby the electrodes have been carried out to improve the efficiency of normal and inverted configuration OSCs [83–92]. In terms of J–V characteristics of normal and inverted configuration OSCs, these improvements correspond to larger shunt resistances and smaller series resistances, leading to an increased FF and eventually high efficiency. The main factors which have influence on the efficiency of cells are: solvent, layer thickness, deposition techniques, size and design, dry time, thermal annealing, substrates, including roughness and resistance [139].

The rapid increases in efficiency of inverted configuration OSCs indicates that the commercially viable efficiencies of greater than 10% should be obtained in the coming years. Solution-processed high work function metal electrodes to replace vacuum-deposited metal electrodes and expensive ITO electrodes and solution processing techniques to deposit the active layers onto flexible substrates in inverted configuration OSCs should favor the feasibility in developing further high efficiency, high lifetime, low-cost, large area, and roll-to-roll printable cells.

Acknowledgement

The authors express their thanks to the supports from the National Natural Science Foundation of China (Grant nos. 10804006, 20904057 and 21074055), the National Natural Science Funds for Distinguished Young Scholar (Grant no. 60825407), Natural Science Foundation of Beijing (Grant no. 1102028), the 111 Project (Grant no.B08002), Basic Research Foundation of Beijing Jiaotong University (2011JBM123) and NUST Research Funding (no. 2010ZDJH04), Beijing Municipal Science & Technology Commission (Z090803044009001), J. Zhang acknowledges financial support by 100 Talents Program of The Chinese Academy of Science, F. Zhang also acknowledges the supports from the "Double Hundred Talents Plan" of Beijing Jiaotong University.

References

[1] J.Y. Kim, K. Lee, N.E. Coates, D. Moses, T.Q. Nguyen, M. Dante, A.J. Heeger, Efficient tandem polymer solar cells fabricated by all-solution processing, Science 317 (2007) 222–225.

[2] S.H. Park, A. Roy, S. Beaupre, S. Cho, N. Coates, J.S. Moon, D. Moses, M. Leclerc, K. Lee, A.J. Heeger, Bulk heterojunction solar cells with internal quantum efficiency approaching 100%, Nat. Photonics 3 (2009) 297–302.

[3] C.S. Kim, L.L. Tinker, B.F. DiSalle, E.D. Gomez, S. Lee, S. Bernhard, Y.L. Loo, Altering the thermodynamics of phase separation in inverted bulk heterojunction organic solar cells, Adv. Mater. 21 (2009) 3110–3115.

[4] D.W. Zhao, L. Ke, Y. Li, S.T. Tan, A.K.K. Kyaw, H.V. Demir, X.W. Sun, D.L. Carroll, G.Q. Lo, D.L. Kwong, Optimization of inverted tandem organic solar cells, Sol. Energy Mater. Sol. Cells 95 (2011) 921–926.

[5] H. Ma, H.L. Yip, F. Huang, A.K.Y. Jen, Interface engineering for organic electronics, Adv. Funct. Mater. 20 (2010) 1371–1388.

[6] P.K. Sudeep, K.T. Early, K.D. McCarthy, M.Y. Odoi, M.D. Barnes, T. Emrick, Monodisperse oligo(phenylene vinylene) ligands on CdSe quantum dots: synthesis and polarization anisotropy measurements, J. Am. Chem. Soc. 130 (2008) 2384–2385.

[7] K.H. Tsai, J.S. Huang, M.Y. Liu, C.H. Chao, C.Y. Lee, S.C. Hung, C.F. Lin, High efficiency flexible polymer solar cells based on PET substrates with a nonannealing active layer, J. Electrochem. Soc. 156 (2009) B1188–B1191.

[8] A. Wicklein, S. Ghosh, M. Sommer, F. Wurthner, M. Thelakkat, Self assembly of semiconductor organogelator nanowires for photoinduced charge separation, ACS Nano 3 (2009) 1107–1114.

[9] H.L. Yip, S.K. Hau, N.S. Baek, H. Ma, A.K.Y. Jen, Polymer solar cells that use self-assembled-monolayer-modified ZnO/Metals as cathodes, Adv. Mater. 20 (2008) 2376–2382.

[10] Y.Y. Lin, T.H. Chu, S.S. Li, C.H. Chuang, C.H. Chang, W.F. Su, C.P. Chang, M.W. Chu, C.W. Chen, Interfacial nanostructuring on the performance of polymer/TiO_2 nanorod bulk heterojunction solar cells, J. Am. Chem. Soc. 131 (2009) 3644–3649.

[11] F.J. Zhang, F.Y. Sun, Y.Z. Shi, Z.L. Zhou, L.F. Lu, D.W. Zhao, Z. Xu, Y.S. Wang, Effect of ultra thin molybdenum trioxide layer and illumination intensity on the performance of organic photovoltaic devices, ACS Energy Fuels 24 (2010) 3739–3742.

[12] F.J. Zhang, Z. Xu, X.J. Liu, S.L. Zhao, L.F. Lu, Y.Sh. Wang, X.R. Xu, Studies on morphology and molecular arrangement of pentacene on different substrates, Superlattice Microstruct. 45 (2009) 612–617.

[13] B. Zimmermann, U. Wurfel, M. Niggemann, Longterm stability of efficient inverted P3HT:PCBM solar cells, Sol. Energy Mater. Sol. Cells 93 (2009) 491–496.

[14] A. Rivaton, S. Chambon, M. Manceau, J.L. Gardette, N. Lamaitre, S. Guillerez, Light-induced degradation of the active layer of polymer-based solar cells, Polym. Degrad. Stabil. 95 (2010) 278–284.

[15] K. Norrman, N.B. Larsen, F.C. Krebs, Lifetimes of organic photovoltaics: combining chemical and physical characterisation techniques to study degradation mechanisms, Sol. Energy Mater. Sol. Cells 90 (2006) 2793–2814.

[16] C. Lungenschmied, G. Dennler, H. Neugebauer, S.N. Sariciftci, M. Glatthaar, T. Meyer, A. Meyer, Flexible, long-lived, large-area, organic solar cells, Sol. Energy Mater. Sol. Cells 91 (2007) 379–384.

[17] K. Norrman, F.C. Krebs, Lifetimes of organic photovoltaics: using TOF-SIMS and $^{18}O_2$ isotopic labelling to characterise chemical degradation mechanisms, Sol. Energy Mater. Sol. Cells 90 (2006) 213–227.

[18] F.C. Krebs, J.E. Carle, N. Cruys-Bagger, M. Andersen, M.R. Lilliedal, M.A. Hammond, S. Hvidt, Lifetimes of organic photovoltaics: photochemistry, atmosphere effects and barrier layers in ITO-MEHPPV: PCBM-aluminium devices, Sol. Energy Mater. Sol. Cells 86 (2005) 499–516.

[19] F.C. Krebs, Air stable polymer photovoltaics based on a process free from vacuum steps and fullerenes, Sol. Energy Mater. Sol. Cells 92 (2008) 715–726.

[20] E.A. Katz, S. Gevorgyan, M.S. Orynbayev, F.C. Krebs, Out-door testing and long-term stability of plastic solar cells, Eur. Phys. J 36 (2006) 307–311.

[21] M. Jorgensen, K. Norrman, F.C. Krebs, Stability/degradation of polymer solar cells, Sol. Energy Mater. Sol. Cells 92 (2008) 686–714.

[22] T. Oyamada, C. Maeda, H. Sasabe, C. Adachi, Efficient electron injection mechanism in organic light-emitting diodes using an ultra thin layer of low-work-function metals, Jpn. J. Appl. Phys. 42 (2003) L1535–L1538.

[23] S.Y. Kim, K. Hong, K. Kim, J.L. Lee, Increase of quantum efficiency in organic light emitting diodes with Mg–Al alloy cathode and RhO_2-coated ITO anode, Electron. Mater. Lett. 4 (2008) 63–66.

[24] H. Kim, M. Shin, J. Park, Y. Kim, Effect of long time annealing and incident light intensity on the performance of polymer: fullerene solar cells, IEEE Trans. Nanotechnol. 9 (2010) 400–406.

[25] M.P. de Jong, L.J. van Ijzendoorn, M.J.A. de Voigt, Stability of the interface between indium-tin-oxide and poly(3,4-ethylenedioxythiophene)/poly(styrenesulfonate) in polymer light-emitting diodes, Appl. Phys. Lett. 77 (2000) 2255–2257.

[26] A. Wan, J. Hwang, F. Amy, A. Kahn, Impact of electrode contamination on the alpha-NPD/Au hole injection barrier, Org. Electron. 6 (2005) 47–54.

[27] M.S. White, D.C. Olson, S.E. Shaheen, N. Kopidakis, D.S. Ginley, Inverted bulk-heterojunction organic photovoltaic device using a solution-derived ZnO underlayer, Appl. Phys. Lett. 89 (2006) 143517.

[28] Z. Xu, L.M. Chen, G.W. Yang, C.H. Huang, J.H. Hou, Y. Wu, G. Li, C.S. Hsu, Y. Yang, Vertical phase separation in poly(3-hexylthiophene): fullerene derivative blends and its advantage for inverted structure solar cells, Adv. Funct. Mater. 19 (2009) 1227–1234.

[29] H.H. Liao, L.M. Chen, Z. Xu, G. Li, Y. Yang, Highly efficient inverted polymer solar cell by low temperature annealing of Cs_2CO_3 interlayer, Appl. Phys. Lett. 92 (2008) 173303.

[30] C.H. Hsieh, Y.J. Cheng, P.J. Li, C.H. Chen, M. Dubosc, R.M. Liang, C.S. Hsu, Highly efficient and stable inverted polymer solar cells integrated with a cross-linked fullerene material as an interlayer, J. Am. Chem. Soc. 132 (2010) 4887–4893.

[31] D. Gupta, S. Mukhopadhyay, K.S. Narayan, Fill factor in organic solar cells, Sol. Energy Mater. Sol. Cells 94 (2010) 1309–1313.

[32] M.C. Scharber, D. Wuhlbacher, M. Koppe, P. Denk, C. Waldauf, A.J. Heeger, C.L. Brabec, Design rules for donors in bulk-heterojunction solar cells—towards 10% energy conversion efficiency, Adv. Mater. 18 (2006) 789–794.

[33] G. Dennler, M.C. Scharber, T. Ameri, P. Denk, K. Forberich, C. Waldauf, C.J. Brabec, Design rules for donors in bulk-heterojunction tandem solar cells-towards 15% energy conversion efficiency, Adv. Mater. 20 (2008) 579–583.

[34] D.M. Nanditha, M. Dissanayake, A.A.D.T. Adikaari, R.J. Curry, R.A. Hatton, S.R.P. Silva, Nanoimprinted large area heterojunction pentacene-C60 photovoltaic device, Appl. Phys. Lett. 90 (2007) 253502.

[35] C.W. Chu, Y. Shao, V. Shrotriya, Y. Yang, Efficient photovoltaic energy conversion in tetracene C60 based heterojunctions, Appl. Phys. Lett. 86 (2005) 243506.

[36] F.T. Reis, D. Mencaraglia, S.O. Saad, I. Seguy, M. Oukachmih, P. Jolinat, P. Destruel, Characterization of ITO/CuPc/AI and ITO/ZnPc/Al structures using optical and capacitance spectroscopy, Synth. Met. 138 (2003) 33–37.

[37] D.Y. Kim, G. Sarasqueta, F. So, SnPc:C60 bulk heterojunction organic photovoltaic cells with MoO_3 interlayer, Sol. Energy Mater. Sol. Cells 93 (2009) 1452–1456.

[38] Y. Yoshida, S. Tanaka, Y. Fujita, I. Hiromitsu, Organic thin film solar cells with a Cu anode: improvement of the photovoltaic properties on aging in air, J. Appl. Phys. 106 (2009) 064510.

[39] I. Kim, H.M. Haverinen, Z.X. Wang, S. Madakuni, Y. Kim, J. Li, G.E. Jabbour, Efficient organic solar cells based on planar metallophthalocyanines, Chem. Mater. 21 (2009) 4256–4260.

[40] Y. Eda, K. Itoh, Y.N. Ito, M. Fujitsuka, T. Majima, T. Kawato, Synthesis and properties of fullerene (C_{70}) complexes of 2,6-bis(porphyrin)-substituted pyrazine derivatives bound to a Pd(II) ion, Supramol. Chem. 22 (2010) 517–523.

[41] M. Ohtani, S. Fukuzumi, Photoelectrochemical cell based on cup-shaped nanocarbon fullerene composite nanocluster film: enhancement of photocurrent generation by cup-shaped nanocarbons as an electron transporter, Fuller Nanot. Carb. Nanostruct. 18 (2010) 251–260.

[42] J. Nishinaga, Y. Horikoshi, Structural properties of C_{60} multivalent metal composite layers grown by molecular beam epitaxy, J. Vac. Sci. Technol. B 28 (2010) C3E10.

[43] H.W. Zhu, J.Q. Wei, K.L. Wang, D.H. Wu, Applications of carbon materials in photovoltaic solar cells, Sol. Energy Mater. Sol. Cells 93 (2009) 1461–1470.

[44] X. Xi, W. Li, J. Wu, J. Ji, Z. Shi, G. Li, A comparative study on the performances of small molecule organic solar cells based on CuPc/C60 and CuPc/C70, Sol. Energy Mater. Sol. Cells 94 (2010) 2435–2441.

[45] F. Cleri, Energy band and vacuum level alignment at a semiconductor–molecule–metal interface, Appl. Phys. Lett. 92 (2008) 103112.

[46] J. Subbiah, D.Y. Kim, M. Hartel, F. So, MoO_3/poly (9,9-dioctylfluorene-co-N-[4-(3-methylpropyl)]-diphenylamine) double-interlayer effect on polymer solar cells, Appl. Phys. Lett. 96 (2010) 063303.

[47] J. Subbiah, P.M. Beaujuge, K.R. Choudhury, S. Ellinger, J.R. Reynolds, F. So, Combined effects of MoO_3 interlayer and $PC_{70}BM$ on polymer photovoltaic device performance, Org. Electron. 11 (2010) 955–958.

[48] M.H. Tong, N.E. Coates, D. Moses, A.J. Heeger, S. Beaupre, M. Leclerc, Charge carrier photogeneration and decay dynamics in the poly(2,7-carbazole) copolymer PCDTBT and in bulk heterojunction composites with $PC_{70}BM$, Phys. Rev. B 81 (2010) 125210.

[49] P. Vemulamada, G. Hao, T. Kietzke, A. Sellinger, Efficient bulk heterojunction solar cells from regio-regular-poly(3,3-didodecyl quaterthiophene)/$PC_{70}BM$ blends, Org. Electron. 9 (2008) 661–666.

[50] F.B. Kooistra, V.D. Mihailetchi, L.M. Popescu, D. Kronholm, P.W.M. Blom, J.C. Hummelen, New C-84 derivative and its application in a bulk heterojunction solar cell, Chem. Mater. 18 (2006) 3068–3073.

[51] R.B. Ross, C.M. Cardona, D.M. Guldi, S.G. Sankaranarayanan, M.O. Reese, N. Kopidakis, J. Peet, B. Walker, G.C. Bazan, E. Van Keuren, B.C. Holloway, M. Drees, Endohedral fullerenes for organic photovoltaic devices, Nat. Mater. 8 (2009) 208–212.

[52] Y.J. He, H.Y. Chen, J.H. Hou, Y.F. Li, Indene-C60 Bisadduct: a new acceptor for high performance polymer solar cells, J. Am. Chem. Soc. 132 (2010) 1377–1382.

[53] S.E. Shaheen, D.S. Ginley, G.E. Jabbour, Organic-based photovoltaics toward low-cost power generation, MRS Bull. 30 (2005) 10–19.

[54] K.M. Coakley, M.D. McGehee, Conjugated polymer photovoltaic cells, Chem. Mater. 16 (2004) 4533–4542.

[55] J. Roncali, Molecular bulk heterojunctions: an emerging approach to organic solar cells, Acc. Chem. Res. 42 (2009) 1719–1730.

[56] C. Kitamura, S. Tanaka, Y. Yamashita, Design of narrow-bandgap polymers. Syntheses and properties of monomers and polymers containing aromatic-donor and o-quinoid-acceptor units, Chem. Mater. 8 (1996) 570–578.

[57] L.J.A. Koster, V.D. Mihailetchi, P.W.M. Blom, Bimolecular recombination in polymer/fullerene bulk heterojunction solar cells, Appl. Phys. Lett. 88 (2006) 052104.
[58] C.J. Brabec, C. Winder, N.S. Sariciftci, J.C. Hummelen, A. Dhanabalan, P.A.v. Hal, R.A.J. Janssen, A low-bandgap semiconducting polymer for photovoltaic devices and infrared emitting diodes, Adv. Funct. Mater. 19 (2002) 709–712.
[59] W. Tang, J. Hai, Y. Dai, Z. Huang, B. Lu, F. Yuan, J. Tang, F. Zhang, Recent development of conjugated oligomers for high efficiency bulk-heterojunction solar cells, Sol. Energy Mater. Sol. Cells 94 (2010) 1963–1979.
[60] N.N. Wang, J.S. Yu, Y. Zang, J. Huang, Y.D. Jiang, Effect of buffer layers on the performance of organic photovoltaic cells based on copper phthalocyanine and C60, Sol. Energy Mater. Sol. Cells 94 (2010) 263–266.
[61] V. Tripathi, D. Datta, G.S. Samal, A. Awasthi, S. Kumar, Role of exciton blocking layers in improving efficiency of copper phthalocyanine based organic solar cells, J. Non-Cryst. Solids 354 (2008) 2901–2904.
[62] M.Y. Chan, C.S. Lee, S.L. Lai, M.K. Fung, F.L. Wong, H.Y. Sun, K.M. Lau, S.T. Lee, Efficient organic photovoltaic devices using a combination of exciton blocking layer and anodic buffer layer, J. Appl. Phys. 100 (2006) 094506.
[63] H.R. Wu, Q.L. Song, M.L. Wang, F.Y. Li, H. Yang, Y. Wu, C.H. Huang, X.M. Ding, X.Y. Hou, Stable small molecule organic solar cells with 1,3,5-tris(2-N-phenylbenzimidazolyl) benzene as an organic buffer, Thin Solid Films 515 (2007) 8050–8053.
[64] X. Tong, B.E. Lassiter, S.R. Forrest, Inverted organic photovoltaic cells with high open-circuit voltage, Org. Electron. 11 (2010) 705–709.
[65] F.J. Zhang, D.W. Zhao, Z.L. Zhuo, H. Wang, Z. Xu, Y.S. Wang, Inverted small molecule organic solar cells with Ca modified ITO as cathode and MoO_3 modified Ag as anode, Sol. Energy Mater. Sol. Cells 94 (2010) 2416–2421.
[66] C. Brabec, V. Dyakonov, J. Parisi, N.S. Sariciftci, Organic Photovoltaics: Concepts and Realization, Springer, Berlin, 2003.
[67] D.W. Zhao, S.T. Tan, L. Ke, P. Liu, A.K.K. Kyaw, X.W. Sun, G.Q. Lo, D.L. Kwong, Optimization of an inverted organic solar cell, Sol. Energy Mater. Sol. Cells 94 (2010) 985–991.
[68] D.W. Zhao, P. Liu, X.W. Sun, S.T. Tan, L. Ke, A.K.K. Kyaw, An inverted organic solar cell with an ultrathin Ca electron-transporting layer and MoO_3 hole-transporting layer, Appl. Phys. Lett. 95 (2009) 153304.
[69] S.K. Hau, H.L. Yip, O. Acton, N.S. Baek, H. Ma, A.K.Y. Jen, Interfacial modification to improve inverted polymer solar cells, J. Mater. Chem. 18 (2008) 5113–5119.
[70] Z.H. Lu, C.C. Lo, C.J. Huang, Y.Y. Yuan, M.W.C. Dharma-wardana, M.Z. Zgierski, Quasimetallic behavior of carrier-polarized C-60 molecular layers: experiment and theory, Phys. Rev. B 72 (2005) 155440.
[71] Z.B. Wang, M.G. Helander, M.T. Greiner, J. Qiu, Z.H. Lu, Energy-level alignment and charge injection at metal/C_{60}/organic interfaces, Appl. Phys. Lett. 95 (2009) 043302.
[72] F.X. Wang, X.F. Qiao, T. Xiong, D.G. Ma, The role of molybdenum oxide as anode interfacial modification in the improvement of efficiency and stability in organic light-emitting diodes, Org. Electron. 9 (2008) 985–993.
[73] J.S. Huang, C.Y. Chou, C.F. Lin, Enhancing performance of organic-inorganic hybrid solar cells using a fullerene interlayer from all-solution processing, Sol. Energy Mater. Sol. Cells 94 (2010) 182–186.
[74] F.C. Krebs, M. Jørgensen, K. Norrman, O. Hagemann, J. Alstrup, T.D. Nielsen, J. Fyenbo, K. Larsen, J. Kristensen, A complete process for production of flexible large area polymer solar cells entirely using screen printing-first public demonstration, Sol. Energy Mater. Sol. Cells 93 (2009) 422–441.
[75] D.A. Rider, B.J. Worfolk, K.D. Harris, A. Lalany, K. Shahbazi, M.D. Fleischauer, M.J. Brett, J.M. Buriak, Stable inverted polymer/fullerene solar cells using a cationic polythiophene modified PEDOT:PSS cathodic interface, Adv. Funct. Mater. 20 (2010) 2404–2415.
[76] L.M. Chen, Z.R. Hong, G. Li, Y. Yang, Recent progress in polymer solar cells: manipulation of polymer:fullerene morphology and the formation of efficient inverted polymer solar cells, Adv. Mater. 21 (2009) 1434–1449.
[77] Y. Gao, H.L. Yip, S.K. Hau, K.M. O'Malley, N.C. Cho, H. Chen, A.K.Y. Jen, Anode modification of inverted polymer solar cells using graphene oxide, Appl. Phys. Lett. 97 (2010) 203306.
[78] A.M. Higgins, S.J. Martin, R.L. Thompson, J. Chappell, M. Voigt, D.G. Lidzey, R.A.L. Jones, M. Geoghegan, Surface segregation and self-stratification in blends of spin-cast polyfluorene derivatives, J. Phys.: Condens. Matter 17 (2005) 1319–1328.
[79] W.H. Baek, T.S. Yoon, H.H. Lee, Y.S. Kim, Composition-dependent phase separation of P3HT:PCBM composites for high performance organic solar cells, Org. Electron. 11 (2010) 933–937.
[80] M. Campoy-Quiles, T. Ferenczi, T. Agostinelli, P.G. Etchegoin, Y. Kim, T.D. Anthopoulos, P.N. Stavrinou, D.D.C. Bradley, J. Nelson, Morphology evolution via self-organization and lateral and vertical diffusion in polymer:fullerene solar cell blends, Nat. Mater. 7 (2008) 158–164.
[81] S.K. Hau, H.L. Yip, N.S. Baek, J.Y. Zou, K. O'Malley, A.K.Y. Jen, Air-stable inverted flexible polymer solar cells using zinc oxide nanoparticles as an electron selective layer, Appl. Phys. Lett. 92 (2008) 253301.
[82] T. Kuwabara, T. Nakayama, K. Uozumi, T. Yamaguchi, K. Takahashi, Highly durable inverted-type organic solar cell using amorphous titanium oxide as electron collection electrode inserted between ITO and organic layer, Sol. Energy Mater. Sol. Cells 92 (2008) 1476–1482.
[83] C. Tao, S.P. Ruan, X.D. Zhang, G.H. Xie, L. Shen, X.Z. Kong, W. Dong, C.X. Liu, W.Y. Chen, Performance improvement of inverted polymer solar cells with different top electrodes by introducing a MoO_3 buffer layer, Appl. Phys. Lett. 93 (2008) 193307.
[84] S.K. Hau, H.L. Yip, H. Ma, A.K.Y. Jen, High performance ambient processed inverted polymer solar cells through interfacial modification with a fullerene self-assembled monolayer, Appl. Phys. Lett. 93 (2008) 233304.
[85] A.K.K. Kyaw, X.W. Sun, C.Y. Jiang, G.Q. Lo, D.W. Zhao, D.L. Kwong, An inverted organic solar cell employing a sol–gel derived ZnO electron selective layer and thermal evaporated MoO_3 hole selective layer, Appl. Phys. Lett. 93 (2008) 221107.
[86] F.C. Krebs, All solution roll-to-roll processed polymer solar cells free from indium-tin-oxide and vacuum coating steps, Org. Electron. 10 (2009) 761–768.
[87] F.C. Krebs, Polymer solar cell modules prepared using roll-to-roll methods: knife-over-edge coating, slot-die coating and screen printing, Sol. Energy Mater. Sol. Cells 93 (2009) 465–475.
[88] F.C. Krebs, S.A. Gevorgyan, J. Alstrup, A roll-to-roll process to flexible polymer solar cells: model studies, manufacture and operational stability studies, J. Mater. Chem. 19 (2009) 5442–5451.
[89] D.J. Baker, C.G. Allen, T.D. Berman, M.R. Bergren, J.M. Albin, D.C. Olson, E.C. Przekwas, M.S. White, D.S. Ginley, R.T. Collins, T.E. Furtak, Functionalized zinc oxide for improved organic photovoltaic systems, in: M. Baldo, P.W.M. Blom, A. Kahn, P. Peumans (Eds.), Physics and Technology of Organic Semiconductor Devices, Materials Research Society, Warrendale, 2010, pp. 143–148.
[90] G. Li, C.W. Chu, V. Shrotriya, J. Huang, Y. Yang, Efficient inverted polymer solar cells, Appl. Phys. Lett. 88 (2006) 253503.
[91] Y. Lee, J.H. Youn, M.S. Ryu, J. Kim, H.T. Moon, J. Jang, Highly efficient inverted poly(3-hexylthiophene): methano-fullerene [6,6]-phenyl C71-butyric acid methyl ester bulk heterojunction solar cell with Cs_2CO_3 and MoO_3, Org. Electron. 12 (2011) 353–357.
[92] S.Y. Sun, T. Salim, L.H. Wong, Y.L. Foo, F. Boey, Y.M. Lam, A new insight into controlling poly(3-hexylthiophene) nanofiber growth through a mixed-solvent approach for organic photovoltaics applications, J. Mater. Chem. 21 (2011) 377–386.
[93] O. Hagemann, M. Bjerring, N.C. Nielsen, F.C. Krebs, All solution processed tandem polymer solar cells based on thermocleavable materials, Sol. Energy Mater. Sol. Cells 92 (2008) 1327–1335.
[94] C.Y. Chou, C.H. Chan, J.S. Huang, C.H. Wu, C.H. Chang, M.Y. Liu, Y.H. Lin, C.F. Lin, Improved performance of polymer/ZnO nanorod hybrid solar cells by slow drying of the photoactive layer, IEEE PV Specialists Conference, Philadelphia, 2009, pp. 2205–2207.
[95] M.R. RajeshMenon, M.V. Maheshkumar, K. Sreekumar, C. SudhaKartha, K.P. Vijayakumar, Inverted polymer solar cells with indium sulfide electron selective layer, Sol. Energy Mater. Sol. Cells 94 (2010) 2212–2217.
[96] T.T. Larsen-Olsen, E. Bundgaard, K.O. Sylvester-Hvid, F.C. Krebs, A solution process for inverted tandem solar cells, Org. Electron. 12 (2011) 364–371.
[97] W.H. Baek, I. Seo, T.S. Yoon, H.H. Lee, C.M. Yun, Y.S. Kim, Hybrid inverted bulk heterojunction solar cells with nanoimprinted TiO_2 nanopores, Sol. Energy Mater. Sol. Cells 93 (2009) 1587–1591.
[98] J.S. Huang, C.Y. Chou, M.Y. Liu, K.H. Tsai, W.H. Lin, C.F. Lin, Solution-processed vanadium oxide as an anode interlayer for inverted polymer solar cells hybridized with ZnO nanorods, Org. Electron. 10 (2009) 1060–1065.
[99] Q.F. Dong, Y.H. Zhou, J.N. Pei, Z.Y. Liu, Y.W. Li, S.Y. Yao, J.B. Zhang, W.J. Tian, All-spin-coating vacuum-free processed semi-transparent inverted polymer solar cells with PEDOT:PSS anode and PAH-D interfacial layer, Org. Electron. 11 (2010) 1327–1331.
[100] C.Y. Chou, J.S. Huang, C.H. Wu, C.Y. Lee, C.F. Lin, Lengthening the polymer solidification time to improve the performance of polymer/ZnO nanorod hybrid solar cells, Sol. Energy Mater. Sol. Cells 93 (2009) 1608–1612.
[101] H. Schmidt, H. Flugge, T. Winkler, T. Bulow, T. Riedl, W. Kowalsky, Efficient semitransparent inverted organic solar cells with indium tin oxide top electrode, Appl. Phys. Lett. 94 (2009) 243302.
[102] T. Kuwabara, H. Sugiyama, M. Kuzuba, T. Yamaguchi, K. Takahashi, Inverted bulk-heterojunction organic solar cell using chemical bath deposited titanium oxide as electron collection layer, Org. Electron. 11 (2010) 1136–1140.
[103] K. Norrman, M.V. Madsen, S.A. Gevorgyan, F.C. Krebs, Degradation patterns in water and oxygen of an inverted polymer solar cell, J. Am. Chem. Soc. 132 (2010) 16883–16892.
[104] R. Søndergaard, M. Helgesen, M. Jørgensen, F.C. Krebs, Fabrication of polymer solar cells using aqueous processing for all layers including the metal back electrode, Adv. Energy Mater. 1 (2011) 68–71.
[105] G. Jo, S.I. Na, S.H. Oh, S. Lee, T.S. Kim, G. Wang, M. Choe, W. Park, J. Yoon, D.Y. Kim, Y.H. Kahng, T. Lee, Tuning of a graphene-electrode work function to enhance the efficiency of organic bulk heterojunction photovoltaic cells with an inverted structure, Appl. Phys. Lett. 97 (2010) 213301.
[106] F.C. Krebs, J. Fyenbo, M. Jørgensen, Product integration of compact roll-to-roll processed polymer solar cell modules: methods and manufacture using flexographic printing, slot-die coating and rotary screen printing, J. Mater. Chem. 20 (2010) 8994–9001.
[107] F.C. Krebs, K. Norrman, Using light-induced thermocleavage in a roll-to-roll process for polymer solar cells, ACS Appl. Mater. Interfaces 2 (2010) 877–887.

[108] K.S. Kim, Y. Zhao, H. Jang, S.Y. Lee, J.M. Kim, K.S. Kim, J.H. Ahn, P. Kim, J.Y. Choi, B.H. Hong, Large-scale pattern growth of graphene films for stretchable transparent electrodes, Nature 457 (2009) 706–710.
[109] M. Hiramoto, M. Suezaki, M. Yokoyama, Effect of thin gold interstitial-layer on the photovoltaic properties of tandem organic solar cell, Chem. Lett. 19 (1990) 327–330.
[110] A. Yakimov, S.R. Forrest, High photovoltage multiple-heterojunction organic solar cells incorporating interfacial metallic nanoclusters, Appl. Phys. Lett. 80 (2002) 1667.
[111] B.P. Rand, J. Genoe, P. Heremans, J. Poortmans, Solar cells utilizing small molecular weight organic semiconductors, Prog. Photovolt. 15 (2007) 659–676.
[112] K. Kawano, N. Ito, T. Nishimori, J. Sakai, Open circuit voltage of stacked bulk heterojunction organic solar cells, Appl. Phys. Lett. 88 (2006) 073514.
[113] J.G. Xue, S. Uchida, B.P. Rand, S.R. Forrest, Asymmetric tandem organic photovoltaic cells with hybrid planar–mixed molecular heterojunctions, Appl. Phys. Lett. 85 (2004) 5757.
[114] A. Hadipour, B. de Boer, J. Wildeman, F.B. Kooistra, J.C. Hummelen, M.G.R. Turbiez, M.M. Wienk, R.A.J. Janssen, P.W.M. Blom, Solution-processed organic tandem solar cells, Adv. Funct. Mater. 16 (2006) 1897–1903.
[115] J. Gilot, I. Barbu, M.M. Wienk, R.A.J. Janssen, The use of ZnO as optical spacer in polymer solar cells: theoretical and experimental study, Appl. Phys. Lett. 91 (2007) 113520.
[116] J. Gilot, M.M. Wienk, R.A.J. Janssen, Double and triple junction polymer solar cells processed from solution, Appl. Phys. Lett. 90 (2007) 143512.
[117] D.W. Zhao, X.W. Sun, C.Y. Jiang, A.K.K. Kyaw, G.Q. Lo, D.L. Kwong, Efficient tandem organic solar cells with an Al/MoO_3 intermediate layer, Appl. Phys. Lett. 93 (2008) 083305.
[118] S. Sista, M.H. Park, Z.R. Hong, Y. Wu, J.H. Hou, W.L. Kwan, G. Li, Y. Yang, Highly efficient tandem polymer photovoltaic cells, Adv. Mater. 22 (2010) 380–383.
[119] X.W. Sun, D.W. Zhao, L. Ke, A.K.K. Kyaw, G.Q. Lo, D.L. Kwong, Inverted tandem organic solar cells with a MoO_3/Ag/Al/Ca intermediate layer, Appl. Phys. Lett. 97 (2010) 053303.
[120] O. Inganas, F.L. Zhang, K. Tvingstedt, L.M. Andersson, S. Hellstrom, M.R. Andersson, Polymer photovoltaics with alternating copolymer/fullerene blends and novel device architectures, Adv. Mater. 22 (2010) E100–E116.
[121] F.J. Zhang, Y. Li, W.H. Tang, J. Wang, X.W. Xu, Z.L. Zhuo, Z. Xu, Y.S. Wang, D. Carroll, Pentacene nanostructural interlayer for the efficiency improvement of polymer solar cells, Thin solid films, in press, doi:10.1016/j.tsf.2010.12.252.
[122] F.J. Zhang, A. Vollmer, J. Zhang, Z. Xu, J.P. Rabe, N. Koch, Energy level alignment and morphology of interfaces between molecular and polymeric organic semiconductors, Org. Electron. 8 (2007) 606–614.
[123] F.C. Krebs, H. Spanggaard, Significant improvement of polymer solar cell stability, Chem. Mater. 17 (2005) 5235–5237.
[124] F.C. Krebs, K. Norrman, Analysis of the failure mechanism for a stable organic photovoltaic during 10000 h of testing, Prog. Photovolt. 15 (2007) 697–712.
[125] A. Seemann, H.J. Egelhaaf, C.J. Brabec, J.A. Hauch, Influence of oxygen on semi-transparent organic solar cells with gas permeable electrodes, Org. Electron. 10 (2009) 1424–1428.
[126] K. Norrman, S.A. Gevorgyan, F.C. Krebs, Water-induced degradation of polymer solar cells studied by $H_2^{18}O$ labeling, ACS Appl. Mater. Interfaces 1 (2009) 102–112.
[127] J.Y. Zou, H.L. Yip, S.K. Hau, A.K.Y. Jen, Metal grid/conducting polymer hybrid transparent electrode for inverted polymer solar cells, Appl. Phys. Lett. 96 (2010) 203301.
[128] S.Y. Park, Y.J. Kang, S. Lee, D.G. Kim, J.K. Kim, J.H. Kim, J.W. Kang, Spray-coated organic solar cells with large-area of 12.25 cm^2, Sol. Energy Mater. Sol. Cells 95 (2011) 852–855.
[129] E. Bundgaard, O. Hagemann, M. Manceau, M. Jørgensen, F.C. Krebs, Low band gap polymers for roll-to-roll coated polymer solar cells, Macromolecules 43 (2010) 8115–8120.
[130] M.R. Lilliedal, A.J. Medford, M.V. Madsen, K. Norrman, F.C. Krebs, The effect of post-processing treatments on inflection points in current–voltage curves of roll-to-roll processed polymer photovoltaics, Sol. Energy Mater. Sol. Cells 94 (2010) 2018–2031.
[131] F.C. Krebs, T. Tromholt, M. Jørgensen, Upscaling of polymer solar cell fabrication using full roll-to-roll processing, Nanoscale 2 (2010) 873–886.
[132] J. Alstrup, M. Jørgensen, A.J. Medford, F.C. Krebs, Ultra fast and parsimonious materials screening for polymer solar cells using differentially pumped slot-die coating, ACS Appl. Mater. Interfaces 2 (2010) 2819–2827.
[133] A.J. Medford, M.R. Lilliedal, M. Jørgensen, D. Aarø, H. Pakalski, J. Fyenbo, F.C. Krebs, Grid-connected polymer solar panels: initial considerations of cost, lifetime, and practicality, Opt. Express 18 (2010) A272–A285.
[134] Y. Galagan, J.J.M. Rubingh, R. Andriessen, C.C. Fan, P.W.M. Blom, S.C. Veenstra, J.M. Kroon, ITO-free flexible organic solar cells with printed current collecting grids, Sol. Energy Mater. Sol. Cells, in press, doi:10.1016/j.solmat.2010.08.011.
[135] F.C. Krebs, T.D. Nielsen, J. Fyenbo, M. Wadstrømc, M.S. Pedersen, Manufacture, integration and demonstration of polymer solar cells in a lamp for the "Lighting Africa" initiative, Energy Environ. Sci. 3 (2010) 512–525.
[136] Konarka Company, 〈http://www.konarka.com〉.
[137] Solarmer Energy, Inc. 〈http://www.solarmer.com/〉.
[138] Heliatek GmbH, 〈http://www.heliatek.com〉.
[139] Y. Galagan, I.G. Vries, A.P. Langen, R. Andriessen, W.J.H..Verhees, S.C..Veenstra, J.M. Kroon, Technology development for roll-to-roll production of organic photovoltaics, Chem. Eng. Process., in press, doi:10.1016/j.cep.2010.07.012.